HHS Public Access

Author manuscript

Sci Immunol. Author manuscript; available in PMC 2022 February 10.

Published in final edited form as:

Sci Immunol. 2021 August 10; 6(62): . doi:10.1126/sciimmunol.abh3567.

Evolution-inspired redesign of the LPS receptor caspase-4 into an interleukin-1β converting enzyme

Pascal Devant[1], **Anh Cao**[1], **Jonathan C. Kagan**[1,2]

[1]Division of Gastroenterology, Boston Children's Hospital and Harvard Medical School, 300 Longwood Avenue, Boston, MA 02115, USA.

Abstract

Innate immune signaling pathways comprise multiple proteins that promote inflammation. This multistep means of information transfer suggests that complexity is a prerequisite for pathway design. Herein, we test this hypothesis by studying caspases that regulate inflammasome-dependent inflammation. Several caspases differ in their ability to recognize bacterial LPS and cleave interleukin-1β (IL-1β). No caspase is known to contain both activities, yet distinct caspases with complementary activities bookend an LPS-induced pathway to IL-1β cleavage. Using caspase-1/4 hybrid proteins present in canines as a guide, we identified molecular determinants of IL-1β cleavage specificity within caspase-1. This knowledge enabled the redesign of human caspase-4 to operate as a one-protein signaling pathway, which intrinsically links LPS detection to IL-1β cleavage and release, independent of inflammasomes. We identified caspase-4 homologues in multiple carnivorans which display the activities of redesigned human caspase-4. These findings illustrate natural signaling pathway diversity and highlight how multistep innate immune pathways can be condensed into a single protein.

One sentence summary

Caspase-4 homologues can naturally evolve or be synthetically engineered to directly link cytosolic LPS detection to IL-1β secretion.

Introduction

Central to our understanding of immunity are the signaling pathways of the innate immune system. Prototypical examples include the pathways activated by the Toll-like Receptors (TLRs) and the Nucleotide binding Leucine Rich Repeat containing (NLR) proteins. Upon detection of microbial products, virulence factors or dysregulation of cellular homeostasis, members of these receptor families seed the assembly of multiprotein complexes known as supramolecular organizing centers (SMOCs; (1)). SMOCs represent the signaling organelles

[2]Correspondence: jonathan.kagan@childrens.harvard.edu.

Author contributions

P.D. designed the study, performed experiments, and wrote manuscript. A.C. generated critical reagents. J.C.K. conceived idea, supervised research, and wrote manuscript. All authors discussed results and commented on manuscript.

Competing interests

J.C.K. holds equity and consults for IFM Therapeutics, Quench Bio and Corner Therapeutics. None of these relationships influenced the work performed in this study. The other authors declare that they have no competing interests.

of the innate immune system, which unleash activities that promote inflammation, interferon responses, changes in metabolism or cell death, in a context-dependent manner. Examples of these signaling organelles include the inflammasomes, which serve as the sites of interleukin-1β (IL-1β) maturation and signals that induce pyroptosis (2).

Inflammasomes are controlled by caspases that operate upstream or downstream of these molecular machines, including caspase-1 (Casp-1), murine Casp-11 (mCasp-11) or human Casp-4 (hCasp-4) and -5 (3). These enzymes consist of an N-terminal caspase activation and recruitment domain (CARD) fused to an enzymatic domain. Upon activation, inflammatory caspases cleave the cytosolic protein gasdermin D (GSDMD), which subsequently forms pores in the plasma membrane that cause lytic cell death (pyroptosis) and the release of the cleaved IL-1 family cytokines IL-1β and IL-18 (4-7).

Despite their commonalities, inflammatory caspases possess protein-specific activities. For example, only Casp-1 has considerable IL-1β converting enzyme (ICE) activity (8) and only Casp-1 can be recruited into inflammasomes to stimulate its catalytic activity (2). mCasp-11, hCasp-4 and -5, in contrast, are not recruited into inflammasomes and their catalytic activity is stimulated by binding of their CARD to bacterial lipopolysaccharide (LPS) (9). As mCasp-11 and hCasp-4 cannot cleave pro-IL-1β, the pathways activated by LPS depend on the downstream activation of the NLRP3 inflammasome. Inflammasome-associated Casp-1 then provides the ICE activity that the upstream caspases cannot (10-12). No caspase is known to combine LPS-binding and IL-1β processing activities. Despite the importance of inflammatory caspases in host defense, the mechanisms underlying their differential cleavage specificities and ligand-binding activities are poorly defined.

Core components of the pyroptosis machinery are conserved throughout vertebrate evolution. Mammals of the order *Carnivora,* including all terrestrial and marine dog-like and cat-like animals, represent an exception to this statement. These animals lack the gene encoding Casp-1 (13, 14). Instead, carnivorans possess a gene where a Casp-1-like CARD is fused to a second CARD and an enzymatic domain, both of which are similar to hCasp-4 (Fig. 1A, B). In addition, transcripts of this gene are spliced to give rise to two isoforms: one that contains a single CARD (Casp-1/4a) and one with both CARDs (Casp-1/4b) (Fig. 1A). Importantly, both carnivoran caspases contain enzymatic domains that are most similar to hCasp-4, which does not contain ICE activity. These bioinformatic observations raise the question of how pyroptosis and IL-1 release is regulated in carnivorans, as key elements of the known pathways are reorganized or missing.

Herein, we show that in contrast to bioinformatic predictions, the Casp-1/4 proteins from *Canis lupus familiaris* display all activities of Casp-1, including the ability to cleave pro-IL-1β. Comparative analysis revealed how mouse and human caspases select pro-IL-1β as a substrate, by a mechanism distinct from that which cleaves GSDMD. This knowledge enabled us to redesign hCasp-4 into a protease exhibiting ICE activity that operated as a one-protein signaling pathway that senses LPS and cleaves IL-1β and GSDMD, independent of inflammasomes. A broader evolutionary analysis revealed multiple animal species that encode a Casp-4 gene whose product naturally operates in a similar manner to our redesigned hCasp-4. These findings reveal molecular determinants of caspase substrate

specificity and challenge the idea that complexity is a prerequisite for innate immune pathway design.

Results

Despite bioinformatic predictions, canine inflammatory caspases are functional homologues of Casp-1.

The gene encoding the inflammasome stimulatory protein NLRP3 is conserved in carnivorans (15). To determine if NLRP3 is operational in carnivoran cells, we primed canine monocyte-derived macrophages (MDMs) (Fig. S1A) with LPS and stimulated with the K^+ ionophore nigericin, an inducer of NLRP3 activation in murine and human cells. Stimulated cells were then stained with the membrane impermeable dye propidium iodide (PI), which binds to intracellular nucleic acids upon plasma membrane disruption, and determined cellular ATP levels as a proxy for viability. Treatments of canine MDMs with nigericin stimulated an increase in PI fluorescence and a decrease in cellular ATP, both of which are indicators of pyroptosis (Fig. 1C and S1B). Nigericin induced these responses in the presence or absence of LPS, as is observed in human monocytes (16). LPS priming correlated with the release of IL-1β (Fig. 1D), which was processed into the bioactive p17 fragment (Fig. 1E; fragment at ~17 kDa). The NLRP3 inhibitor MCC950 (17) prevented nigericin-induced cell death, as cells treated with this inhibitor exhibited lower PI staining and higher ATP levels, as compared to non-inhibitor-treated cells (Fig. 1C, Fig. S1B). In addition, the pan-caspase inhibitor zVAD-FMK and disulfiram, an inhibitor of GSDMD pore formation (18), reduced nigericin-induced death. (Fig. 1C, Fig. S1B). All three inhibitors diminished IL-1β release (Fig. 1D). Overall, these data indicate that the NLRP3 inflammasome pathway is intact in canine cells.

Our finding that IL-1β can be cleaved and released from canine MDMs was notable, as Casp-1 is missing in dogs. To explain these findings, we determined if canine Casp-1/4 (cCasp-1/4a and cCasp-1/4b) proteins can operate as Casp-1. We designed an experimental system based on stable, heterologous expression of a caspase in immortalized bone marrow-derived macrophages (iBMDMs) from mice deficient in mCasp-1 and mCasp-11 (hereafter referred to as *Casp-1/11*$^{-/-}$ iBMDMs). We reconstituted *Casp-1/11*$^{-/-}$ iBMDMs with cCasp-1/4 isoforms (cCasp-1/4a or cCasp-1/4b), mCasp-1, mCasp-11, or hCasp-4. cCasp-1/4a and cCasp-1/4b could be detected by immunoblot using a Casp-4-specific, but not a Casp-1-specific, antibody, underscoring their identity as structural Casp-4 homologues (Fig. 1F).

We primed cells with LPS and subsequently stimulated with nigericin. Within wild type (WT) cells, these treatments induced pyroptosis, as assessed by the release of the cytosolic enzyme lactate dehydrogenase (LDH) and IL-1β (Fig. 1G). Both processes were abrogated in *Casp-1/11*$^{-/-}$ iBMDMs expressing GFP or mCasp-11 as a transgene, but were restored by expression of mCasp-1 (Fig. 1G). Similar to mCasp-1, cells expressing cCasp-1/4a or cCasp1/4b released LDH and IL-1β upon LPS priming and nigericin treatment. These phenotypes coincided with the cleavage of GSDMD into its pore-forming N-terminal domain (Fig. 1H). Similar results were obtained when cells were transfected with poly(dA:dT) (Fig. S1C, D), which stimulates the AIM2 inflammasome (19, 20).

Poly(dA:dT)-induced LDH release was independent of LPS priming (Fig. S1C), as expected (19).

In addition to stimulating pyroptosis, select inflammasome activators can induce IL-1β release from living (hyperactive) cells (21, 22). Infection of macrophages with *S. aureus* lacking O-acetyltransferase A (SA113 Δ*oatA*) causes hyperactivation in a Casp1-dependent manner (22). We infected transgene-expressing *Casp-1/11*$^{-/-}$ iBMDMs with SA113 Δ*oatA*. WT iBMDMs, as well as cells expressing mCasp-1, cCasp-1/4a or cCasp-1/4b responded to infection with the release of IL-1β, but not LDH, and the amount of IL-1β could be boosted if cells were primed with LPS (Fig. 1I). No IL-1β was released from *Casp-1/11*$^{-/-}$ iBMDMs expressing GFP or mCasp-11 upon infection (Fig. 1I).

Within mCasp-1, the N-terminal CARD is critical for recruitment into inflammasomes (23, 24). To determine the role of the CARD within cCARD-1/4a and cCARD1/4b, we reconstituted *Casp-1/11*$^{-/-}$ iBMDMs with a canine caspase construct lacking its Casp-1-like CARD. Cells expressing this mutant caspase (cCasp-1/4bΔCARD) failed to release LDH or IL-1β after LPS priming followed by nigericin treatment (Fig. S1E-H). These collective data demonstrate that both cCasp-1/4 isoforms can operate similar to Casp-1 in the context of multiple inflammasome stimuli.

Canine caspases are not LPS sensors and canine cells cannot respond to intracellular LPS.

While the first CARD of cCasp-1/4b is similar to that of Casp-1, the second CARD shares homology with the LPS-sensing CARDs of hCasp-4 and mCasp-11. We therefore investigated whether cCasp-1/4b might respond to exposure to LPS. Transgenic cells were primed with LPS before delivery of LPS into the cytosol via electroporation. LPS electroporation stimulated LDH release from WT iBMDMs and *Casp-1/11*$^{-/-}$ iBMDMs expressing mCasp-11 or hCasp-4, indicating the induction of pyroptosis (Fig. 2A). Cells expressing mCasp-1 or GFP did not lyse upon LPS electroporation. Notably, none of our reconstituted *Casp-1/11*$^{-/-}$ iBMDMs released significant amounts of IL-1β after LPS electroporation (Fig. 2B). This finding validates current dogma, which predicts that mCasp-11 and mCasp-1 are both needed for LPS to induce cleavage and release IL-1β (11). Since our iBMDMs produce either mCasp-1 or mCasp-11 (not both), IL-1β release is diminished.

We found that neither cCasp-1/4a nor cCasp-1/4b expressing cells died upon cytosolic LPS delivery (Fig. 2A). These results imply that cCasp-1/4b cannot become activated by LPS. To further investigate this lack in LPS responsiveness, we determined if the Casp-4-like CARD from cCasp-1/4b can functionally replace the LPS-sensing CARD from either mCasp-11 or hCasp-4. We designed chimeric caspases where the CARDs from cCasp-1/4b were attached to the enzymatic domain from mCasp-11 (mEnz11) or hCasp-4 (hEnz4) (cCARD1+4/mEnz11 and cCARD1+4/hEnz4). These chimeric proteins were stably produced in *Casp-1/11*$^{-/-}$ iBMDMs (Fig. 2C, D). Cells expressing these chimeras failed to promote pyroptosis when electroporated with LPS (Fig. 2E). We further considered the possibility that the Casp-1-like CARD prevents LPS detection by cCasp-1/4b. However, deletion of this additional CARD did not render cells responsive to LPS electroporation

(Fig. S2A). Even within primary canine MDMs, we observed no evidence of cell death or IL-1β release upon LPS electroporation (Fig. 2F-H). Altering electroporation conditions did not reveal any LPS-specific changes in canine MDMs (Fig. S2B-D). In human and pig monocytes (but not MDMs), the TLR4 pathway activates the NLRP3 inflammasome to promote IL-1β release (25). We observed similar responses when we stimulated canine monocytes with LPS, as these treatments promoted IL-1β release (Fig. S2E, F). Canine cells are therefore not generally unresponsive to LPS but are specifically unresponsive to cytosolic LPS.

Canine caspase activities reveal distinct mechanisms of IL-1β and GSDMD substrate selection by murine and human inflammatory caspases.

Our findings suggest that cCasp-1/4 proteins operate most similarly to Casp-1 homologues in humans and mice. We therefore investigated mechanisms that underlie this symmetry of activities. Cysteine 285 (C285) is the main catalytic residue within human and murine Casp-1 (26), which is conserved in the canine caspases. We introduced Cys-to-Ala mutations at the equivalent sites in cCasp-1/4a and cCasp-1/4b (C285A and C370A, respectively) and expressed these mutants in *Casp-1/11*$^{-/-}$ iBMDMs (Fig. 3A). We did not observe any LDH release, secretion of IL-1β, or processing of GSDMD after LPS + nigericin treatment of cells expressing these cCasp-1/4 mutants (Fig. 3B-F). The catalytic activity of cCasp-1/4a and cCasp-1/4b is therefore required to induce pyroptosis and IL-1β release.

The ability of cCasp-1/4 proteins to induce IL-1β processing was surprising, as their catalytic domain is most similar to that found in hCasp-4, a caspase that has minimal ICE activity (27, 28). The presence of cleaved IL-1β in the supernatants of the reconstituted macrophages could be explained if Casp-4 homologues actually do have ICE activity, but this activity is dormant under natural conditions and can only be stimulated upon recruitment into an inflammasome.

To address this possibility, we created a scenario whereby the enzymatic domains of hCasp-4 or mCasp-11 can be recruited into inflammasomes via a mechanism similar to Casp-1. This was accomplished by generating fusions between the CARD of hCasp-1 or mCasp-1 to full-length hCasp-4 or mCasp-11, or the isolated enzymatic domains of these caspases (Fig. 3G). When expressed in *Casp-1/11*$^{-/-}$ iBMDMs, these chimeric enzymes caused a similar degree of pyroptosis after LPS + nigericin treatment (Fig. 3H, I). However, this pyroptotic cell death was not accompanied by the release of mature IL-1β (Fig. 3J, K). These findings eliminate the possibility that recruitment of hCasp-4 or mCasp-11 into an inflammasome stimulates a latent ICE activity.

Based on the above-described phenotypes, we considered the possibility that cCasp-1/4 display intrinsic ICE properties. We therefore purified recombinant catalytic domains from mCasp-1, hCasp-4 and cCasp-1/4. Analysis by SDS-PAGE confirmed that the recombinant enzymes are autocatalytically processed into the large (p20) and small (p10) catalytic subunits (Fig. 4A). We then characterized their ability to cleave peptide-based and full-length protein substrates. Enzyme kinetic analyses using YVAD-pNA, a chromogenic tetrapeptide substrate optimized for cleavage by Casp-1, revealed similar Michaelis-Menten constants (K_m) for mCasp-1 and cCasp-1/4, while the K_m of hCasp-4 for this substrate was

so high it was not possible to calculate (Fig. 4B, C). The turnover number (k_{cat}) and catalytic efficiency of mCasp-1 were only 2-3-fold higher than those of cCasp-1/4 (Fig. 4C). Similar results were observed when we examined whether the can caspases process pro-IL-1β. As expected, pro-IL-1β was cleaved far more efficiently by mCasp-1 than by hCasp-4 (Fig. 4D, E). Our results are consistent with earlier reports that hCasp-4 can process pro-IL-1β *in vitro*, albeit at very slow rates, which imply that this reaction is unlikely to be of physiological relevance (29). Intriguingly, cCasp-1/4 processed murine pro-IL-1β at a near-comparable rate to mCasp-1 (Fig. 4F, G). Equivalent results were obtained when the canine variant of this cytokine was used as a substrate (Fig. S3A-D). We also investigated the ability of our recombinant caspases to process another IL-1 family member, pro-IL-18 (30). As expected (28, 31), mCasp-1 and hCasp-4 efficiently cleaved pro-IL-18 and produced the mature 18 kDa fragment (p18) and cCasp-1/4 cleaved pro-IL-18 with a similar efficiency (Fig. S3E-H). These findings demonstrate that cCasp-1/4 enzymes can process IL-1 family cytokines comparably to mCasp-1.

To identify the molecular determinants for the ICE activity of cCasp-1/4, we first generated chimeric enzymes consisting of the p20 domain of cCasp-1/4 and the p10 domain of hCasp-4, and vice versa. Both chimeras exhibited intermediate catalytic efficiencies of pro-IL-1β cleavage (Fig. S4A-C). This finding suggests that sites distributed across the large and small subunit contribute to pro-IL-1β cleavage, with sites in the small subunit being dominant.

We reasoned that critical residues should be conserved among carnivoran Casp-1/4 homologues, but not in hCasp-4. By applying this rationale, we identified several conserved residues (E288/P290, H342, K345, K379) in cCasp-1/4, which we individually replaced with the respective amino acids from hCasp-4. Each of the single point mutations (E288A/P290R, H342D, K345M, K379T) led to a slight decrease in cleavage efficiency compared to WT cCasp-1/4 (Fig. 4H). When combining three (triple mutant: H342D, K345M, and K379T) or four of the mutations (quadruple mutant), we observed additive effects, causing pro-IL-1β cleavage efficiency to drop to a level similar to hCasp-4 (Fig. 4H, Fig. S4E-J). Notably, the ability of the quadruple mutant to cleave GSDMD remained unaffected, indicating a specific impact of the mutations on cleavage of pro-IL-1β, without affecting the overall activity of the caspase (Fig. 4H, Fig. S4K). Introduction of reciprocal canine-specific mutations into hCasp-4 had the opposite effect. While individual point mutations led to modest increases (~4-6-fold) in the ability to cleave pro-IL-1β, by combining mutations at several sites we generated a hCasp-4 quadruple mutant, which is as efficient as cCasp-1/4 at processing pro-IL-1β (Fig. 4I, Fig. S5A-H). We observed only minor effects of these mutations on GSDMD cleavage (Fig. 4I). Consistent with these findings, the cCasp-1/4 triple mutant maintained the ability to support LPS + nigericin induced pyroptosis when expressed in *Casp-1/11*$^{-/-}$ iBMDMs (Fig. 4J, K). In this situation, however, cell lysis was not accompanied by the release of mature IL-1β (Fig. 4L, M). These findings therefore identify amino acids that determine ICE activity in human and canine caspases.

When mapping the amino acids of interest onto a homology model of cCasp-1/4 in complex with the peptide inhibitor zVAD-FMK, we found that the conserved positively charged residues H342, K345 and K379 are located in the same region in the p10 subunit: a cleft

formed by two loops proximal to the tetrapeptide binding site (Fig. S5I). This charged site is spatially distinct from the hydrophobic recognition site for GSDMD (highlighted in yellow in Fig. S5I)(32, 33). This observation suggests that positive charges in this cavity promote recognition of pro-IL-1β as a cleavage substrate. To test this model, we created additional caspases carrying charge reversal mutations within this region. A D381R mutation in cCasp-1/4 increased its ability to cleave pro-IL-1β by 4-fold (Fig. S6A, B), whereas a R354D mutation in hCasp-4 further decreased its cleavage efficiency by 10-fold (Fig. S6A, C). Similar to its canine counterpart, mCasp-1 E379R was ~3-fold better at cleaving pro-IL-1β than WT mCasp-1 (Fig. S6A, D).

H342 drew our attention, as it is positioned in a manner that suggests a direct involvement in coordinating the tetrapeptide in the active site (Fig. S5I). H342 is present in most carnivoran Casp-1/4 proteins and is conserved in Casp-1. Casp-4 homologues that contain no ICE activity, such as hCasp-4, display a negative charge at this site (Fig. S6E). Introducing a charge-swap H340D mutation into mCasp-1 greatly decreased its ability to process pro-IL-1β, while only slightly affecting GSDMD cleavage (~31-fold and ~2-fold reduction compared to WT mCasp-1, respectively) (Fig. 5A, Fig. S6F-H). To determine if this cleavage deficiency extended to activities within cells, we reconstituted *Casp-1/11*$^{-/-}$ iBMDMs with a mCasp-1 H340D mutant (Fig. 5B). After LPS + nigericin treatment, we detected less processed IL-1β released from cells expressing mCasp-1 H340D, as compared to WT mCasp-1-expressing cells (Fig. 5C, D). LDH release, GSDMD processing and autocatalytic cleavage of mCasp-1 H340D were unimpaired, indicating an IL-1β-specific effect of the H340D mutation (Fig. 5E-G). We confirmed these results in cells expressing hCasp-1 (or the respective H340D mutant), thereby establishing the importance of H340 across species (Fig. 5H-K). These collective findings establish that the charge of amino acids within the catalytic site determines ICE activity, but has minimal impact on the GSDMD-cleaving activity of inflammatory caspases.

Recognition and cleavage of GSDMD is mediated by hydrophobic interactions between a conserved protease exosite present in the L2 loop region of all inflammatory caspases and the C-terminal domain of GSDMD (32, 33)(Fig. S7A). We investigated if mutations in this site affect the ability of a caspase to process pro-IL-1β. We generated cCasp-1/4 and mCasp-1 mutants in which the exosite has been disrupted by introducing a hydrophilic side chain (cCasp-1/4 W294N, mCasp-1 L294N). cCasp-1/4 W294N and mCasp-1 L294N exhibited a marked decrease in the ability to process GSDMD compared to their WT counterparts (Fig. S7B, C). In contrast, we observed only weak effects on pro-IL-1β cleavage (~40 vs. 4-fold reduction; Fig. S7B, D). Overall, these data suggest that recognition of GSDMD and pro-IL-1β are mediated by spatially and functionally distinct regions of the caspase.

Redesign of hCasp-4 to intrinsically link LPS detection to IL-1β cleavage and release, without the need for inflammasomes

In mice, mCasp-11 and mCasp1 link LPS detection to the release of IL-1β, with inflammasomes serving as an intermediate between these enzymes. Based on the finding that we can redesign hCasp-4 into an enzyme with the ability to process IL-1β *in vitro,*

it should be possible to condense the natural multistep LPS-mediated pathway to IL-1β release into one single protein. To fulfill this task, hCasp-4 would need to exhibit LPS-sensing, GSDMD and IL-1β cleavage functionalities. As a proof of concept of this idea, we first designed chimeric caspases consisting of the LPS-binding CARDs from hCasp-4 or mCasp-11 and the enzymatic domain of cCasp-1/4 (named hCARD4/cEnz and mCARD11/cEnz, respectively). These chimeric enzymes were expressed in *Casp-1/11*$^{-/-}$ iBMDMs (Fig. 6A, Fig. S8A). Cells expressing either caspase underwent pyroptosis, as assessed by LDH release after LPS electroporation (Fig. 6B, C). Cells expressing either chimeric caspase also released higher amounts of IL-1β, as compared to cells expressing WT caspases (Fig. 6D, E). Notably, the cleaved p17 fragment of IL-1β was exclusively detected in the supernatants of cells expressing hCARD4/cEnz or mCARD11/cEnz, but not of cells expressing hCasp-4 or mCasp-11 (Fig. 6F, G). The ability of these chimeric caspases to promote IL-1β cleavage and release was independent of NLRP3, as production of this cytokine was insensitive to NLRP3 inhibition by MCC950 (Fig. 6H, I, Fig. S8B, C). In contrast, MCC950 prevented IL-1β release (but not LDH release) from WT iBMDMs after LPS electroporation (Fig. S8D, E), as expected (10). These findings demonstrate that caspases can be engineered to bypass the need for inflammasomes to promote IL-1β cleavage and release.

To determine if the chimera-based strategy of inflammasome-bypass can be extended to a subtler engineering approach, we examined the redesigned hCasp-4 quadruple mutant that displays ICE activity *in vitro*. Within *Casp-1/11*$^{-/-}$ cells expressing this LPS receptor, which contains only four amino acid substitutions, LPS electroporation stimulated IL-1β and LDH release. In contrast, cells expressing WT hCasp-4 released LDH, but not IL-1β (Fig. 6J-L). Consistent with IL-1β release by redesigned hCasp-4 being an inflammasome-independent process, IL-1β release was insensitive to MCC950 (Fig. 6K,L). To further verify that redesigned hCasp-4 could bypass inflammasomes and cleave and release IL-1β, we determined if these cells could respond to LPS + nigericin treatment. Consistent with the fact that these cells lack endogenous mCasp-1 and mCasp-11, LPS + nigericin treatment was unable to promote IL-1β release (Fig. S8F, G). Thus, IL-1β cleavage after LPS electroporation is driven by the intrinsic activities of redesigned hCasp-4, independent of inflammasomes.

We investigated whether this inflammasome-independent pathway can be engaged by Gram-negative bacteria. We focused on *Salmonella enterica* serovar Typhimurium, which activates inflammasomes by mCasp-11, NLRP3 and NAIP-NLRC4 (34). We eliminated NLRP3 activities from consideration in these studies, as the iBMDMs used are unresponsive to NLRP3 agonists. In addition, we used a flagellin-deficient strain of *Salmonella* (SL1344 *fliC/fljB*) (35) to diminish NAIP-NLRC4 inflammasome activities (36). Consistent with this experimental setup focusing attention on LPS-induced activities, infection with SL1344 *fliC/fljB* induced LDH release in a hCasp-4 or mCasp-11 transgene-dependent manner (Fig. 6N, O). Consistent with our findings with electroporated LPS, infection-induced IL-1β release was strongly enhanced within cells expressing redesigned caspases that contain LPS-binding and ICE activity (hCasp-4 quadruple mutant, hCARD4/cEnz or mCARD11/cEnz) (Fig. 6P-S). In contrast, cells expressing WT hCasp-4 or mCasp-11 were unable to release cleaved IL-1β after infection (Fig. 6R, S). These collective data demonstrate the redesign

of a normally inflammasome-dependent process into a one-protein signaling pathway that intrinsically links LPS detection to IL-1β cleavage and release.

Multiple animal species encode a one-protein signaling pathway that bypasses inflammasomes to link LPS detection with IL-1 cleavage and release.

Our finding that the inflammasome pathway can be bypassed by the simple introduction of four mutations into hCasp-4 raises the question of whether similar caspases and pathways exist in nature. To address this possibility, we performed a cell-based mini-screen, where we introduced Casp-4 homologues from species spanning a range of mammalian orders (namely mouse, cat, lemur, rabbit, sheep, horse, bat, manatee and wombat) into *Casp-1/11*$^{-/-}$ iBMDMs (Fig. 7A). We electroporated cells with LPS and assessed IL-1β release and pyroptosis. With the exception of the manatee and wombat genes, all Casp-4 homologues responded to LPS electroporation with the induction of pyroptosis (Fig. 7B). The observation that manatee and wombat Casp-4 do not support LPS-induced pyroptosis is interesting, as these species are evolutionarily most distant from the rest of the animals in our panel. This finding hints that recognition of LPS might not be a primordial function of Casp-4, but was acquired after these species diverged. Another caspase that stands out is the Casp-4 homologue from the cat (feline Casp-1/4b). Unlike other caspases examined, *Casp-1/11*$^{-/-}$ iBMDMs expressing feline Casp-1/4b released large amounts of mature IL-1β (Fig. 7C, D). As observed with our synthetically redesigned pathways, IL-1β release induced by feline Casp-1/4b was insensitive to MCC950 (Fig. 7E). Feline primary MDMs behaved in a similar manner: When LPS was delivered to the cytosol, pyroptosis and the release of mature IL-1β was evident. Unlike in murine iBMDMs, MCC950 cotreatment did not inhibit IL-1β processing and secretion (Fig. 7F). We eliminated the possibility that MCC950 is ineffective in feline cells, as it inhibited cell death and IL-1β release when NLRP3 was activated by nigericin (Fig. 7G). These findings suggests that IL-1β is processed and secreted upon activation of feline Casp-1/4b by LPS, without the need for inflammasomes. Intrigued by the apparent dichotomy in the behavior of canine and feline Casp-1/4b, we characterized Casp-4 homologues from additional carnivoran species. When introduced into *Casp-1/11*$^{-/-}$ iBMDMs, most caspases examined, including those found in carnivorous and herbivorous bears (polar bear, panda), marine pinnipeds (harbor seal), and diverse felines (tiger, cheetah) conferred the ability to cause LDH and IL-1β release in response to LPS electroporation (Fig. 7H). The only exceptions in this panel were made by Casp-4 homologues from dingo and fox which, like the common dog, are members of the *Canidae* family. These proteins failed to respond to intracellular LPS (Fig. 7H). When we correlated our functional analyses with their evolutionary relationship, we could divide the examined Casp-4 homologues into three distinct classes: Class 1, represented by mCasp-11 and hCasp-4, are Casp-4 homologues, which sense LPS, but do not exhibit ICE activity; Class 2, which includes most carnivoran Casp-1/4 proteins, both sense LPS and have ICE activity; Class 3 is represented by Casp-1/4 proteins from canines, which have ICE activity, but are unresponsive to LPS. Most carnivorans, but not dogs and closely related species, therefore have the ability to mount an inflammatory response to cytosolic LPS, and they do so by employing a natural one-protein signaling pathway (Fig. S9).

Discussion

In this study, we discovered that bioinformatic alignments failed to accurately predict the functions of cCasp-1/4 enzymes. Whereas one of the CARDs in cCasp-1/4b is similar to LPS-sensing CARDs, cCasp-1/4b does not recognize LPS and canine cells do not respond to cytosolic LPS. Similarly, the enzymatic domains within cCasp-1/4 closely resemble that from hCasp-4, yet cCasp-1/4 proteins display ICE activity *in vitro* and within cells. Based on this evidence, we propose that cCasp-1/4 proteins represent functional homologues of Casp-1. We speculate that such bioinformatic—function disconnects may become more common, as it is increasingly recognized that each species has tailored its immune networks in different manners (37).

We demonstrate that carnivoran caspases are excellent tools to identify general mechanisms of substrate selection by inflammatory caspases. Our analysis revealed that the ability of cCasp-1/4 and its murine and human counterparts to cleave pro-IL-1β is conferred by a small set of charged amino acids located in proximity to the active site. These findings highlight how ICE activity is conferred to select caspases, which is a process distinct from that which facilitates GSDMD cleavage. We suggest a model whereby an overall positive electrostatic potential in or in close proximity to the caspase active site promotes pro-IL-1β cleavage. In line with this model, H340 in mCasp-1 is the only conserved positively charged amino acid near its active site. Mutation of H340D results in a 30-fold decrease in ICE activity (Fig. 5A). In contrast, H342 in cCasp-1/4 is proximal to other charged residues (*e.g.* K345 and K379) all of which are conserved in carnivorans. Mutation of all these residues is necessary to abolish ICE activity (Fig. 4H). This model can also explain why feline Casp-1/4, which lacks H342, but contains other positively charged amino acids adjacent to the active site, exhibits ICE activity (Fig. 7, Fig. S4D). Nevertheless, we cannot exclude that additional interactions might play a role in the recognition of pro-IL-1β by specific caspases, particularly mCasp-1, which exhibited superior catalytic activity in our assays.

A notable aspect of the mutations we identified is that they appear to specifically affect ICE activity, rather than overall catalytic activity of the caspase. In contrast, a recent study identified mutations that are conserved in some species of bats that dampen the inflammatory capacity of Casp-1 (38). However, these mutations most likely inhibit Casp-1 homodimerization, thereby interfering not only with IL-1β processing, but also cleavage of GSDMD and Casp-1 itself.

The knowledge gained from the study of canine caspases not only identified molecular determinants of ICE activity within Casp-1, but also illustrated the plasticity of network design. Our data indicate a direct correlation between the ability of a caspase to cleave pro-IL-1β *in vitro* and the degree to which it promotes IL-1β release from a cell, independent of the cell biological path that leads to its activation. While we found that artificial recruitment of the enzymatic domains of hCasp-4 or mCasp-11 into an inflammasome does not promote IL-1β processing, a caspase with ICE activity will cause IL-1β release, no matter if its activation was inflammasome-dependent or initiated by an interaction with LPS. We exploited this relationship to design synthetic one-protein signaling pathways that intrinsically link LPS detection to IL-1β cleavage and release via GSDMD, bypassing

the need for an inflammasome. Strikingly, we discovered that similar pathways naturally exist in multiple animal species. This simplified means of signal propagation contrasts with the complex pathway architecture that is commonly observed in human and mouse innate immunity. While complex pathways allow for intricate ways to regulate signal transduction (39), multistep processes might also offer more opportunities for pathogens to develop immune evasive strategies. The synthetic and natural one-protein signaling pathways we described reveal unexpected network-design flexibility, which provides a mandate to investigate the potential cost and benefits of different types of innate immune pathway design.

Materials and Methods

Study design

The aim of this study was to investigate Casp-1/4 fusion proteins found in carnivoran mammals and use them as a tool to obtain general insights into inflammatory caspase substrate selection. We investigated the function of these enzymes *in vitro* using recombinant proteins, in reconstituted murine macrophages and feline and canine primary cells. Sample sizes for each experiment are indicated in the figure legends.

Cell lines

All cells were cultured in humidified incubators at 37°C and 5% CO_2. Immortalized bone marrow-derived macrophages (iBMDMs) from WT or *Casp-1/11*$^{-/-}$ mice were cultured in DMEM supplemented with 10% fetal bovine serum (FBS), Penicillin + Streptomycin, L-Glutamine and Sodium pyruvate, herafter referred to as complete DMEM (cDMEM). cDNA sequences for wildtype or chimeric caspase constructs of interest carrying an N-terminal Myc-tag were ordered as gBlocks (Integrated DNA technologies) and cloned into pMSCV IRES EGFP using *NotI* and *SalI* restriction sites. Point mutations were introduced using the Quikchange mutagenesis kit (Agilent) or the Q5 mutagenesis kit (NEB) according to manufacturer's protocols. All constructs generated in this paper were sequence confirmed by Sanger sequencing. HEK293T cells were cultured in cDMEM and used as packaging cells for retroviral vectors. For the production of retroviral particles, 2.5x10^6 HEK293T cells were seeded in a 10 cm cell culture dish. After overnight incubation at 37°C, cells were transfected with 10 μg of pMSCV IRES EGFP encoding the protein of interest, 6 μg of pCL-ECO and 3 μg of pCMV-VSVG using Lipofectamine 2000 (ThermoFisher) according to the manufacturer's instructions. After 18-24 h at 37°C, media was changed to 6 ml of fresh cDMEM and virus containing supernatant was collected 24 h post media change. Supernatants were clarified from cellular debris by centrifugation (400 x g, 5 min) and filtered through a 0.45 μm PVDF syringe filter. ~2x10^6 Caspase-1/11$^{-/-}$ iBMDMs were transduced twice on two consecutive days in a 6-well plate by adding 4.5 ml of viral supernatant supplemented with Polybrene (1:2000; EMD Millipore) per well, followed by centrifugation for 1 h at 1250 x g and 30 °C. GFP$^+$ cells were sorted twice on a FACSAria or FACSMelody cell sorter (BD Biosciences) to obtain cell lines with stable and homogenous expression of the target protein. Transgene expression was confirmed by immunobloting using a rabbit anti-Myc-tag or mouse anti-Myc-tag primary antibody (both from Cell Signaling Technologies) at a 1:1000 dilution.

Primary cell culture

Canine or feline whole blood from healthy beagle dogs was purchased from BioIVT and processed within 24 h post blood draw. Primary cells were cultured in RPMI supplemented with 10% FBS, L-Glutamine, Sodium pyruvate and Penicillin + Streptomycin (referred to as complete RPMI). Whole blood was diluted at a 1:1 ratio with sterile PBS pH 7.4 + 2.5 mM EDTA before layering 30 ml of diluted blood over 15 ml of FiColl Paque PLUS density gradient media (GE Healthcare). Density gradient centrifugation was performed at 800 x g for 35 min at 20 °C. Total peripheral blood mononuclear cells were havested from the interphase and washed twice with wash buffer (PBS pH 7.4, 2.5 mM EDTA, 1% FBS). Red blood cells were lysed by resuspending the pellet in ACK lysis buffer and incubation for 5 – 10 min at RT. After a final washing step in wash buffer, total PBMCs were seeded in T75 cell culture flasks in 15 ml complete RPMI ($40x10^6$ PBMCs per flask). After incubation for 2 h at 37°C for canine PBMCs or overnight for feline PBMCs, non-adherent PBMCs were removed by three washes with pre-warmed, sterile PBS pH 7.4. Adherent cells (monocytes) were either used for experiments right away or cultured in complete RPMI supplemented with 50 ng/ml of recombinant human M-CSF (R&D Systems) for 5-7 days. Media was replenished with fresh complete RPMI containing M-CSF every 2 – 3 days.

Differentiation and immortalization of bone marrow-derived macrophages

Bone marrow-derived macrophages were immortalized as described before with slight modifications (40). L929 fibroblasts secreting M-CSF were cultured in cDMEM and M-CSF containing supernatants were harvested, cleared by centrifugation (400 x g, 5 min) and passed through a 0.22 μm filter. CreJ2 cells were cultured in cDMEM and J2 retrovirus-containing supernatans were harvested, cleared by centrifugation (400 x g, 5 min) and passed through a 0.45 μm filter. Femurs from freshly sacrificed *Casp-1/11*$^{-/-}$ mice (B6N.129S2-Casp1tm1Flv/J from Jackson Laboratories) were dissected and flushed with sterile PBS pH 7.4. Obtained cell suspension was passed through a 70 μm cell strainer before plating cells in non-tissue culture-treated 10 cm dishes (1×10^7 cells per dish). Cells were cultured in cDMEM supplemented with 30% M-CSF-containing supernatants from L929 cells for 4 days. On day 4 and 6 post isolation, bone marrow cells were transduced with J2 virus by swapping media for immortalization media (30% L929 supernatant + 70% CreJ2 supernatant) for 24 h. Following day 7, cells were passaged in cDMEM supplemented with gradually decreasing doses of L929 conditioned media (starting at 30%) until they divided normally in unsupplemented cDMEM. When the concentration of supplemented L929 supernatant was below 5%, cells were cultured tissue culture-treated plates for better adherence.

Ligand and chemical reconstitution

E. coli LPS (serotype O:111 B4) was purchased from Enzo Biosciences as a ready-to-use stock solution of 1 mg/ml and used at a working concerntration of 1 μg/ml. Nigericin was bought from Invivogen, dissolved in 100% ethanol to 6.7 mM and used for NLRP3 stimulation at a concentration of 10 μM. Poly(dA:dT) was from Invivogen and dissolved to a stock concentration of 1 mg/ml. Poly(dA:dT) was transfected at a final concentration of 5 μg/ml. MCC950 and zVAD-FMK (both from Invivogen) were resuspended in sterile

DMSO to a concentration of 20 mM and used at a final concentration of 10 μM and 20 μM, respectively. Disulfiram was purchased from Tocris Biosciences, dissolved in DMSO to generate a stock solution at 20 mM. During inhibition experiments, disulfiram was present at a concentration of 50 μM. To inhibit pyroptosis, cells were pre-treated with inhibitors for 30 min and the respective inhibitor was present during signal 2 of inflammasome stimulation. Propidium iodide solution (1 mg/ml) was purchased from MilliporeSigma. Recombinant human M-CSF (CHO expressed, carrier-free) was bought from R&D Systems and dissolved in sterile PBS pH 7.4 (stock concentration 50 μg/ml). YVAD-pNA was from Enzo Biosciences and the stock solution was prepared at 20 mM in DMSO.

Inflammasome activation, cell death assays and ELISAs

Inflammasome activation assays were performed in a 96-well format. To activate the NLRP3 inflammasome, 1 x 10^5 cells were seeded in duplicate wells in 100 μl of cDMEM and incubated for 1 h at 37°C and 5% CO_2 for cells to adhere to the plate before adding 100 μl of cDMEM with or without 2x LPS (1 μg/ml final concentration) for priming. After 4 h at 37°C and 5% CO_2, cells were stimulated with 10 μM nigericin in 200 μl cDMEM for 3 h. Cell lysis was quantified using the CyQuant LDH cytotoxicity assay kit (Thermo Fisher). 50 μl of supernatants were mixed with 50 μl of LDH assay buffer and incubated for 15 – 30 min at RT. Absorbance at 490 nm and 680 nm was meaured on a Tecan Spark plate reader and signal was normalized to lysis controls. Since primary cells yielded low signal intensities in LDH assays, PI staining was used as a readout to quantify membrane perforation in experiments involving these cells. 1 x 10^5 canine cells or 0.5 x 10^5 feline cells were treated as described in a black 96-well plate with clear bottom and PI was added to the media at a 1:300 dilution 30 min before the end of the stimulation. Plates were spun for 5 min at 400 x g and fluorescence was measured on a Tecan Spark device at an excitation wavelength of 530 nm and an emission wavelength of 617 nm. Cellular ATP levels as a measure of viability were determined using the Celltiter-Glo Luminescent Cell Viability kit (Promega). Supernatant was completely removed from the cells stimulated in a 96-well format before adding 30 μl of Opti-MEM and 30 μl of Celltiter-Glo solution per well. After incubation for 5 min at RT, the mixture was transferred into a white 96-well plate and luminescence signal was quantified using a Tecan Spark device. Release of IL-1β was assessed by ELISA using the IL1 beta mouse uncoated ELISA kit (Thermo Fisher), or the feline or canine IL-1 beta/IL1F2 DuoSet kit (both from R&D Systems), respectively, according to manufacturer's protocols. To activate the AIM2 inflammasome, 5 x 10^4 cells were seeded in duplicate wells in 100 μl of cDMEM and incubated overnight at 37°C and 5% CO_2. After priming with 1 μg/ml of LPS for 4 h, cells were transfected with 5 μg/ml of Poly(dA:dT) (Inivivogen) using Lipofectamine 2000 in a total volume of 200 μl cDMEM per well. Supernatants for LDH assay and ELISA analysis were collected 6 h post-transfection.

Processing of GSDMD and caspase-1 after inflammasome activation was analyzed by immunoblotting using a rabbit anti-GSDMD (Abcam) or mouse anti-murine caspase-1 p20 (Adipogen) primary antibodies; diluted at 1:1000. 1 – 2 x 10^6 iBMDMs of the cell line of interest were seeded in a 6-well plate and primed with 1 μg/ml of LPS for 3 – 4 h. In order to capture proteins present in the lysate and the supernatant, nigericin was administered in 1.5

ml of Opti-MEM media for 2 h. Samples for immunoblotting were prepared by adding 375 µl of 5x SDS loading buffer directly to the well and heated to 65 °C for 10 min.

LPS electroporation

The Neon transfection system (ThermoFisher) was used to deliver bacterial LPS into the cytoplasm of cells. Canine MDMs or murine iBMDMs cells primed with LPS for 3 - 4 h in 6-well plates, lifted with PBS + EDTA and resuspended in R buffer at a density of 10 x 10^6 cell/ml. Feline MDMs were primed equivalently in non-TC-treated 6-well plates and resuspended in R buffer at a density between 3 - 5 x 10^6 cell/ml. LPS or sterile PBS (negative control) was mixed with the cell supension (1 µg of LPS or 1 ul of PBS per 1 x 10^6 cells, respectively) before aspirating the cell suspension into the electroporation pipette equipped with a 100 µl tip and performing electroporation with two pulses with a width of 10 ms and a voltage of 1400 V, unless stated otherwise. Cells were then dispensed into media at a density of 5 x 10^5 cell/ml (murine and canine cells) or 2.5 x 10^5 cell/ml (feline cells) and seeded in 96-well (200 µl per well) or 6-well tissue culture plates. Cell death and IL-1β release was quantified 3 h post-electroporation by LDH or PI and CelltiterGlo assay, and ELISA.

Bacterial infections

S. aureus strain lacking the *oatA* gene (SA113 Δ*oatA*) was a kind gift from David Underhill (Cedars Sinai). Bacteria were streaked on TSA agar plates containing sheep blood (Thermo Fisher) and incubated overnight at 37°C. Single colonies were picked to inoculate 5 ml of Todd-Hewitt Broth (Millipore Sigma) containing 25 µg/ml of kanamycin and grown up at 37°C and 250 rpm for 24 h. Cultures were washed three times in PBS pH 7.4, and OD_{600} was determined before appropriately diluting bacteria in cDMEM without antibiotics. 1 x 10^5 iBMDMs per well in a 96-well plate were primed with 1 µg/ml LPS or left untreated followed by infection with SA113 Δ*oatA* at an MOI of 30 in a total volume of 200 µl per well. Synchronized infection was facilitated by spinning the plates at 500 x g for 5 min right after addition of bacteria-containing media. After 1 h of infection, extracellular bacteria were killed by changing the media to cDMEM (with Pen/Strep) and supplemented with 50 µg/ml of gentamicin. Cell culture supernatants for LDH release assay and ELISA to quantify levels of IL-1β in the were collected 12 h post initial infection.

Salmonella strain deficient for flagellin (SL1344 *fliC/fljB*) was a kind gift from Igor Brodsky (University of Pennsylvania) and infections were performed as described before with minor modifications (35). Bacteria were streaked on LB agar plates containing 25 µg/ml kanamycin, grown overnight at 37°C and plates were stored at 4 °C for later use. Overnight cultures (3 ml LB + 25 µg/ml kanamycin and 25 µg/ml chloramphenicol) were inoculated with a single bacterial colony and grown at 37°C while shaking at 250 rpm. On the next morning, bacterial culture was diluted into high salt LB (3 ml LB + 100 µl of overnight culture + 78 µl of sterile 5 M NaCl) and incubated for another 3 h at 37°C without shaking. Infections were performed in a 96-well (for LDH and ELISA analyses) or 12-well format (for IL-1β immunoprecipitations) using 1x10^5 and 1x10^6 cells per well, respectively. Cells were seeded in cDMEM without Pen/Strep and primed with 1 µg/ml of LPS for 3 h. Bacteria were washed three times with pre-warmed cDMEM without Pen/Strep and added to

cells at an MOI of 100 in 200 µl (96-well) or 2 ml (12-well) of cDMEM without Pen/Strep. Synchronized infection was facilitated by spinning the plates at 500 x g for 5 min right after addition of bacteria-containing media and cells were incubated at 37°C and 5 % CO_2. After 1 h, gentamicin was added to a final concentration of 100 µg/ml to kill extracellular bacteria. Cell culture supernatants for downstream analyses were harvested at 4 h post-infection.

Immunoprecipitation of IL-1β from cell culture supernatants

IP of murine IL-1β from cell culture supernatants was performed as described before (7). Supernatants from 0.5 – 1.0 x 10^6 cells (cell number consistent within each individual experiment) stimulated as indicated were transferred into 5 ml FACS tubes and depleted of cells and debris by spinning at 400 x g for 5 min. Cell-free supernatants were transferred into new tubes and rotated overnight at 4 °C in the presence of 0.5 µg of biotinylated goat anti-murine IL-1β antibody (R&D Systems) and 20 µl neutravidin agarose beads (Thermo Fisher). Remaining cells in the well were lysed in 1x SDS loading dye and served as input control. Beads were subsequently washed three times with PBS pH 7.4 before eluting bound proteins in 50 µl of 1x SDS loading dye. Immunoprecipitated and cell-associated IL-1β was detected by immunoblotting using a rabbit anti-murine IL-1β antibody (Genetex). Cell-associated actin or tubulin was detected as a loading control using a mouse anti-tubulin antibody (DSHB hybridoma bank; 1:100 dilution) or a mouse anti-actin antibody from Sigma at a dilution of 1:5000. IP of canine or feline IL-1β was performed equivalently from pooled supernatants from two wells of a 96-well plate containing 0.5 – 1.0 x 10^5 cells per well using 0.18 µg of biotinylated canine/feline IL-1β ELISA detection antibody (R&D Systems) as bait and rabbit anti-canine IL-1β antibody from BioRad or goat anti-feline IL-1β antibody from R&D Systems for immunoblot detection. Unless stated otherwise, all primary antibodies were used at a concentration of 1:1000.

Recombinant protein expression and purification

DNA sequences encoding residues 131 - 404 of canine caspase-1/4 isoform a, residues 94 - 377 of human caspase-4 and residues 130 – 404 of murine caspase-1 were amplified by PCR using gBlocks of the full-length proteins as a template and cloned into a pET28A(+) vector with an N-terminal His_6-tag using *BamHI* and *EcoRI* restriction sites. cDNA encoding full-length murine pro-IL-1β, canine pro-IL-1β and human pro-IL-18 was synthesized by Integrated DNA Technologies and cloned equivalently. Chemically competent Rosetta (DE3) pLysS cells (EMD Millipore) were transformed with the plasmid of interest and plated on LB agar plates with 25 µg/ml of Kanamycin. Overnight pre-cultures inoculated with a single colony were grown at 30 °C and 250 rpm in 2x YT media containing 25 µg/ml kanamycin and 50 µg/ml chloramphenicol. Expression cultures of 500 – 1500 ml were inoculated with overnight cultures at a ratio of 1:100 and incubated at 37°C and 250 rpm until the OD_{600} reached a value between 0.7 and 0.8. Following a cooling step on ice, protein expression was induced by adding IPTG to a final concentration of 0.25 mM and expression was allowed to proceed overnight at 18 °C. Bacterial pellets were harvested by centrifugation (5000 x g for 20 – 30 min at 4 °C) and stored at −20 °C if not immediately used for protein purification.

To purify recombinant proteins, bacterial pellets were resuspended in resuspension buffer (25 mM HEPES-NaOH pH 7.4, 150 mM NaCl, 10 mM Imidazole) and lysed by

ultrasonication. Cell lysates were clarified by centrifugation (30 min, 20,000 x g, 4 °C) and passed through a 0.22 μm syringe filter before pouring them into a gravity flow column containing a bed of Ni-NTA agarose beads (Qiagen). Beads were washed with at least 10 bed volumes of wash buffer (25 mM HEPES pH 7.4, 400 mM NaCl, 25 mM Imidazole) and bound protein was eluted stepwise in resuspension buffer supplemented with 40 – 250 mM Imidazole. Fractions containing the protein of interest were pooled, buffer exchanged into storage buffer (25 mM HEPES-NaOH pH 7.4, 150 mM NaCl, 10% glycerol) using a PD-10 desalting column (GE Healthcare). Lastly, protein was concentrated by centrifugal ultrafiltration. Aliquots were snap-frozen in liquid nitrogen and stored at −80 °C for later use. Purity and integrity of the purified proteins were analyzed by SDS-PAGE followed by Instant*Blue* staining (Expedeon).

Recombinant human GSDMD was provided by Hao Wu (Harvard Medical School) and purified as described (18).

In vitro protein substrate cleavage assays

Two-fold dilution series of the indicated recombinant caspase were incubated with purified murine/canine pro-IL-1β, human pro-IL-18 or human GSDMD at a final concentration of 50 nM in 40 μl of caspase buffer (10 mM PIPES pH 7.2, 10% sucrose, 10 mM DTT, 100 mM NaCl, 1 mM EDTA, 0.1% CHAPS) for 30 min at 37°C. Reactions were stopped by adding 15 μl of 5x SDS loading dye and boiling at 65 °C for 10 min. Cleavage products were analyzed via immunoblot using rabbit anti-murine IL-1β (Genetex), rabbit anti-human IL-18 (MBL), or rabbit anti-GSDMD (Cell Signaling) primary antibody at a 1:1000 dilution. Band intensities were quantified using ImageJ to determine EC50 values and catalytic efficiencies were calculated as described before (8) using the following equation:

$$\frac{k_{cat}}{K_m} = \frac{\ln(2)}{(EC_{50} \times t)}$$

In vitro peptide cleavage assays

For peptide cleavage assays, recombinant mCasp-1, hCasp-4 or cCasp-1/4 were first diluted to a concentration of 100 nM in caspase assay buffer. To start the reaction, 20 μl of the diluted caspase were then mixed with 80 μl of a serial dilution of the chromogenic tetrapeptide substrate YVAD-pNA in the same buffer (final concentration of caspase was 20 nM in a total volume of 100 μl) in a clear 96-well plate. Absorbance at a wavelength of 405 nm was measured every 20 s for 20 min using a Tecan Spark plate reader with temperature control set to 37°C. Substrate solution was pre-warmed to 37°C before adding to the caspase to ensure homogenous assay conditions. Absorbance values were plotted in dependence of time and initial velocities were determined by performing linear fits of the resulting curves. A pNA standard curve was generated to transform absorbance values into molar concentrations. Initial velocities were plotted as a function of the substrate concentration and kinetic parameters (K_m, V_{max}, k_{cat}) were determined by performing a fit according to the Michaelis-Menten equation in GraphPad Prism.

Sequence alignments and homology modelling

Mammalian caspase homologues were identified by NCBI BLASTp search using amino acid sequences of canine Casp-1/4a or human Casp-1 as search queries. Sequences of interest were aligned using the Clustal Omega Multiple Sequences Alignment tool and visualized in ESPript 3.0 (41, 42).

To generate a homology model of the catalytic domain of cCasp-1/4, we utilized tools available on the SWISS-MODEL online server (43). A crystal structure of the catalytic domain of human Casp-1 in complex with the inhibitor zVAD-FMK (sequence identity 57% and 63% for the p20 and p10 fragment, respectively) was used as an input template (PDB ID: 2H51)(44). Obtained homology model was visualized in PyMOL (Schroedinger, Inc.).

Quantification and Statistical Analysis

Statistical significance was determined by two-way ANOVA or one-way ANOVA with Tukey's multiple comparison test, or unpaired, two-tailed Student's t-test as appropriate for each experimental dataset. Utilized statistical method is indicated in the respective figure legends. P-values below 0.05 were seen as statistically significant. All statistical analyses were performed using GraphPad Prism data analysis software. Data is representative of at least three independent repeats. Data with error bars are represented as mean ± standard error of the mean.

Data and Materials Availability

All data needed to evaluate the conclusions in the paper are in the paper or Supplementary Materials. Further information and requests for resources and reagents should be directed to and will be fulfilled by the lead contact, Jonathan C. Kagan.

Supplementary Material

Refer to Web version on PubMed Central for supplementary material.

Acknowledgments

We thank Igor Brodsky for providing flagellin-deficient *Salmonella* and Hao Wu for providing purified GSDMD. Cell sorting was performed at the Harvard Immunology Flow Cytometry Core Facility or the Harvard Digestive Disease Center Flow Cytometry Core Facility. We thank members for the Kagan lab for helpful discussions.

Funding

This work was supported by NIH grants AI133524, AI093589, AI116550 and P30DK34854 to J.C.K. J.C.K. holds an Investigators in the Pathogenesis of Infectious Disease Award from the Burroughs Wellcome Fund. P.D. is supported by a fellowship by the Boehringer Ingelheim Fonds.

References and Notes

1. Kagan JC, Magupalli VG, Wu H, SMOCs: supramolecular organizing centres that control innate immunity. Nat. Rev. Immunol 14, 821–6 (2014). [PubMed: 25359439]
2. Schroder K, Tschopp J, The inflammasomes. Cell. 140, 821–32 (2010). [PubMed: 20303873]
3. Kesavardhana S, Malireddi RKS, Kanneganti T-D, Caspases in Cell Death, Inflammation, and Pyroptosis. Annu. Rev. Immunol 38, 567–595 (2020). [PubMed: 32017655]

4. Shi J, Zhao Y, Wang K, Shi X, Wang Y, Huang H, Zhuang Y, Cai T, Wang F, Shao F, Cleavage of GSDMD by inflammatory caspases determines pyroptotic cell death. Nature. 526, 660–665 (2015). [PubMed: 26375003]
5. Kayagaki N, Stowe IB, Lee BL, O'Rourke K, Anderson K, Warming S, Cuellar T, Haley B, Roose-Girma M, Phung QT, Liu PS, Lill JR, Li H, Wu J, Kummerfeld S, Zhang J, Lee WP, Snipas SJ, Salvesen GS, Morris LX, Fitzgerald L, Zhang Y, Bertram EM, Goodnow CC, Dixit VM, Caspase-11 cleaves gasdermin D for non-canonical inflammasome signalling. Nature. 526, 666–671 (2015). [PubMed: 26375259]
6. Liu X, Zhang Z, Ruan J, Pan Y, Magupalli VG, Wu H, Lieberman J, Inflammasome-activated gasdermin D causes pyroptosis by forming membrane pores. Nature. 535, 153–8 (2016). [PubMed: 27383986]
7. Evavold CL, Ruan J, Tan Y, Xia S, Wu H, Kagan JC, The Pore-Forming Protein Gasdermin D Regulates Interleukin-1 Secretion from Living Macrophages. Immunity. 48, 35–44.e6 (2018). [PubMed: 29195811]
8. Ramirez MLG, Poreba M, Snipas SJ, Groborz K, Drag M, Salvesen GS, Extensive peptide and natural protein substrate screens reveal that mouse caspase-11 has much narrower substrate specificity than caspase-1. J. Biol. Chem 293, 7058–7067 (2018). [PubMed: 29414788]
9. Shi J, Zhao Y, Wang Y, Gao W, Ding J, Li P, Hu L, Shao F, Inflammatory caspases are innate immune receptors for intracellular LPS. Nature. 514, 187–192 (2014). [PubMed: 25119034]
10. Baker PJ, Boucher D, Bierschenk D, Tebartz C, Whitney PG, D'Silva DB, Tanzer MC, Monteleone M, Robertson AAB, Cooper MA, Alvarez-Diaz S, Herold MJ, Bedoui S, Schroder K, Masters SL, NLRP3 inflammasome activation downstream of cytoplasmic LPS recognition by both caspase-4 and caspase-5. Eur. J. Immunol 45, 2918–2926 (2015). [PubMed: 26173988]
11. Rühl S, Broz P, Caspase-11 activates a canonical NLRP3 inflammasome by promoting K + efflux. Eur. J. Immunol 45, 2927–2936 (2015). [PubMed: 26173909]
12. Schmid-Burgk JL, Gaidt MM, Schmidt T, Ebert TS, Bartok E, Hornung V, Caspase-4 mediates non-canonical activation of the NLRP3 inflammasome in human myeloid cells. Eur. J. Immunol 45, 2911–7 (2015). [PubMed: 26174085]
13. Eckhart L, Ballaun C, Hermann M, VandeBerg JL, Sipos W, Uthman A, Fischer H, Tschachler E, Identification of Novel Mammalian Caspases Reveals an Important Role of Gene Loss in Shaping the Human Caspase Repertoire. Mol. Biol. Evol 25, 831–841 (2008). [PubMed: 18281271]
14. Eckhart L, Ballaun C, Uthman A, Gawlas S, Buchberger M, Fischer H, Tschachler E, Duplication of the caspase-12 prodomain and inactivation of NLRC4/IPAF in the dog. Biochem. Biophys. Res. Commun 384, 226–30 (2009). [PubMed: 19394309]
15. Cui H, Zhang L, Key Components of Inflammasome and Pyroptosis Pathways Are Deficient in Canines and Felines, Possibly Affecting Their Response to SARS-CoV-2 Infection. Front. Immunol 11 (2021), doi:10.3389/fimmu.2020.592622.
16. Gritsenko A, Yu S, Martin-Sanchez F, Diaz-del-Olmo I, Nichols E-M, Davis DM, Brough D, Lopez-Castejon G, Priming Is Dispensable for NLRP3 Inflammasome Activation in Human Monocytes In Vitro. Front. Immunol 11 (2020), doi:10.3389/fimmu.2020.565924.
17. Coll RC, Robertson AAB, Chae JJ, Higgins SC, Muñoz-Planillo R, Inserra MC, Vetter I, Dungan LS, Monks BG, Stutz A, Croker DE, Butler MS, Haneklaus M, Sutton CE, Núñez G, Latz E, Kastner DL, Mills KHG, Masters SL, Schroder K, Cooper MA, O'Neill LAJ, A small-molecule inhibitor of the NLRP3 inflammasome for the treatment of inflammatory diseases. Nat. Med 21, 248–255 (2015). [PubMed: 25686105]
18. Hu JJ, Liu X, Xia S, Zhang Z, Zhang Y, Zhao J, Ruan J, Luo X, Lou X, Bai Y, Wang J, Hollingsworth LR, Magupalli VG, Zhao L, Luo HR, Kim J, Lieberman J, Wu H, FDA-approved disulfiram inhibits pyroptosis by blocking gasdermin D pore formation. Nat. Immunol 21, 736–745 (2020). [PubMed: 32367036]
19. Hornung V, Ablasser A, Charrel-Dennis M, Bauernfeind F, Horvath G, Caffrey DR, Latz E, Fitzgerald KA, AIM2 recognizes cytosolic dsDNA and forms a caspase-1-activating inflammasome with ASC. Nature. 458, 514–8 (2009). [PubMed: 19158675]
20. Fernandes-Alnemri T, Yu J-W, Datta P, Wu J, Alnemri ES, AIM2 activates the inflammasome and cell death in response to cytoplasmic DNA. Nature. 458, 509–13 (2009). [PubMed: 19158676]

21. Zanoni I, Tan Y, Di Gioia M, Broggi A, Ruan J, Shi J, Donado CA, Shao F, Wu H, Springstead JR, Kagan JC, An endogenous caspase-11 ligand elicits interleukin-1 release from living dendritic cells. Science. 352, 1232–6 (2016). [PubMed: 27103670]
22. Wolf AJ, Reyes CN, Liang W, Becker C, Shimada K, Wheeler ML, Cho HC, Popescu NI, Coggeshall KM, Arditi M, Underhill DM, Hexokinase Is an Innate Immune Receptor for the Detection of Bacterial Peptidoglycan. Cell. 166, 624–636 (2016). [PubMed: 27374331]
23. Stehlik C, Lee SH, Dorfleutner A, Stassinopoulos A, Sagara J, Reed JC, Apoptosis-associated speck-like protein containing a caspase recruitment domain is a regulator of procaspase-1 activation. J. Immunol 171, 6154–63 (2003). [PubMed: 14634131]
24. Srinivasula SM, Poyet J-L, Razmara M, Datta P, Zhang Z, Alnemri ES, The PYRIN-CARD protein ASC is an activating adaptor for caspase-1. J. Biol. Chem 277, 21119–22 (2002). [PubMed: 11967258]
25. Gaidt MM, Ebert TS, Chauhan D, Schmidt T, Schmid-Burgk JL, Rapino F, Robertson AAB, Cooper MA, Graf T, Hornung V, Human Monocytes Engage an Alternative Inflammasome Pathway. Immunity. 44, 833–46 (2016). [PubMed: 27037191]
26. Wilson KP, Black J-AF, Thomson JA, Kim EE, Griffith JP, Navia MA, Murcko MA, Chambers SP, Aldape RA, Raybuck SA, Livingston DJ, Structure and mechanism of interleukin-lβ converting enzyme. Nature. 370, 270–275 (1994). [PubMed: 8035875]
27. Faucheu C, Diu A, Chan AW, Blanchet AM, Miossec C, Hervé F, Collard-Dutilleul V, Gu Y, Aldape RA, Lippke JA, A novel human protease similar to the interleukin-1 beta converting enzyme induces apoptosis in transfected cells. EMBO J. 14, 1914–22 (1995). [PubMed: 7743998]
28. Bibo-Verdugo B, Snipas SJ, Kolt S, Poreba M, Salvesen GS, Extended subsite profiling of the pyroptosis effector protein gasdermin D reveals a region recognized by inflammatory caspase-11. J. Biol. Chem 295, 11292–302 (2020). [PubMed: 32554464]
29. Kamens J, Paskind M, Hugunin M, Talanian RV, Allen H, Banach D, Bump N, Hackett M, Johnston CG, Li P, Identification and characterization of ICH-2, a novel member of the interleukin-1 beta-converting enzyme family of cysteine proteases. J. Biol. Chem 270, 15250–6 (1995). [PubMed: 7797510]
30. Dinarello CA, Novick D, Kim S, Kaplanski G, Interleukin-18 and IL-18 Binding Protein. Front. Immunol 4 (2013), doi:10.3389/fimmu.2013.00289.
31. Wandel MP, Kim B-H, Park E-S, Boyle KB, Nayak K, Lagrange B, Herod A, Henry T, Zilbauer M, Rohde J, MacMicking JD, Randow F, Guanylate-binding proteins convert cytosolic bacteria into caspase-4 signaling platforms. Nat. Immunol (2020), doi:10.1038/s41590-020-0697-2.
32. Liu Z, Wang C, Yang J, Chen Y, Zhou B, Abbott DW, Xiao TS, Caspase-1 Engages Full-Length Gasdermin D through Two Distinct Interfaces That Mediate Caspase Recruitment and Substrate Cleavage. Immunity. 53, 106–114.e5 (2020). [PubMed: 32553275]
33. Wang K, Sun Q, Zhong X, Zeng M, Zeng H, Shi X, Li Z, Wang Y, Zhao Q, Shao F, Ding J, Structural Mechanism for GSDMD Targeting by Autoprocessed Caspases in Pyroptosis. Cell. 180, 941–955.e20 (2020). [PubMed: 32109412]
34. Doerflinger M, Deng Y, Whitney P, Salvamoser R, Engel S, Kueh AJ, Tai L, Bachem A, Gressier E, Geoghegan ND, Wilcox S, Rogers KL, Garnham AL, Dengler MA, Bader SM, Ebert G, Pearson JS, De Nardo D, Wang N, Yang C, Pereira M, Bryant CE, Strugnell RA, Vince JE, Pellegrini M, Strasser A, Bedoui S, Herold MJ, Flexible Usage and Interconnectivity of Diverse Cell Death Pathways Protect against Intracellular Infection. Immunity. 53, 533–547.e7 (2020). [PubMed: 32735843]
35. Wynosky-Dolfi MA, Snyder AG, Philip NH, Doonan PJ, Poffenberger MC, Avizonis D, Zwack EE, Riblett AM, Hu B, Strowig T, Flavell RA, Jones RG, Freedman BD, Brodsky IE, Oxidative metabolism enables Salmonella evasion of the NLRP3 inflammasome. J. Exp. Med 211, 653–668 (2014). [PubMed: 24638169]
36. Rauch I, Deets KA, Ji DX, von Moltke J, Tenthorey JL, Lee AY, Philip NH, Ayres JS, Brodsky IE, Gronert K, Vance RE, NAIP-NLRC4 Inflammasomes Coordinate Intestinal Epithelial Cell Expulsion with Eicosanoid and IL-18 Release via Activation of Caspase-1 and -8. Immunity. 46, 649–659 (2017). [PubMed: 28410991]

37. Daugherty MD, Malik HS, Rules of Engagement: Molecular Insights from Host-Virus Arms Races. Annu. Rev. Genet 46, 677–700 (2012). [PubMed: 23145935]

38. Goh G, Ahn M, Zhu F, Lee LB, Luo D, Irving AT, Wang L-F, Complementary regulation of caspase-1 and IL-1β reveals additional mechanisms of dampened inflammation in bats. Proc. Natl. Acad. Sci 117, 28939–28949 (2020). [PubMed: 33106404]

39. Lee MJ, Yaffe MB, Protein Regulation in Signal Transduction. Cold Spring Harb. Perspect. Biol 8, a005918 (2016). [PubMed: 27252361]

40. De Nardo D, Kalvakolanu DV, Latz E, Immortalization of Murine Bone Marrow-Derived Macrophages. Methods Mol. Biol 1784, 35–49 (2018). [PubMed: 29761386]

41. Madeira F, mi Park Y, Lee J, Buso N, Gur T, Madhusoodanan N, Basutkar P, Tivey ARN, Potter SC, Finn RD, Lopez R, The EMBL-EBI search and sequence analysis tools APIs in 2019. Nucleic Acids Res. 47, W636–W641 (2019). [PubMed: 30976793]

42. Robert X, Gouet P, Deciphering key features in protein structures with the new ENDscript server. Nucleic Acids Res. 42, W320–4 (2014). [PubMed: 24753421]

43. Waterhouse A, Bertoni M, Bienert S, Studer G, Tauriello G, Gumienny R, Heer FT, de Beer TAP, Rempfer C, Bordoli L, Lepore R, Schwede T, SWISS-MODEL: homology modelling of protein structures and complexes. Nucleic Acids Res. 46, W296–W303 (2018). [PubMed: 29788355]

44. Datta D, Scheer JM, Romanowski MJ, Wells JA, An Allosteric Circuit in Caspase-1. J. Mol. Biol 381, 1157–1167 (2008). [PubMed: 18590738]

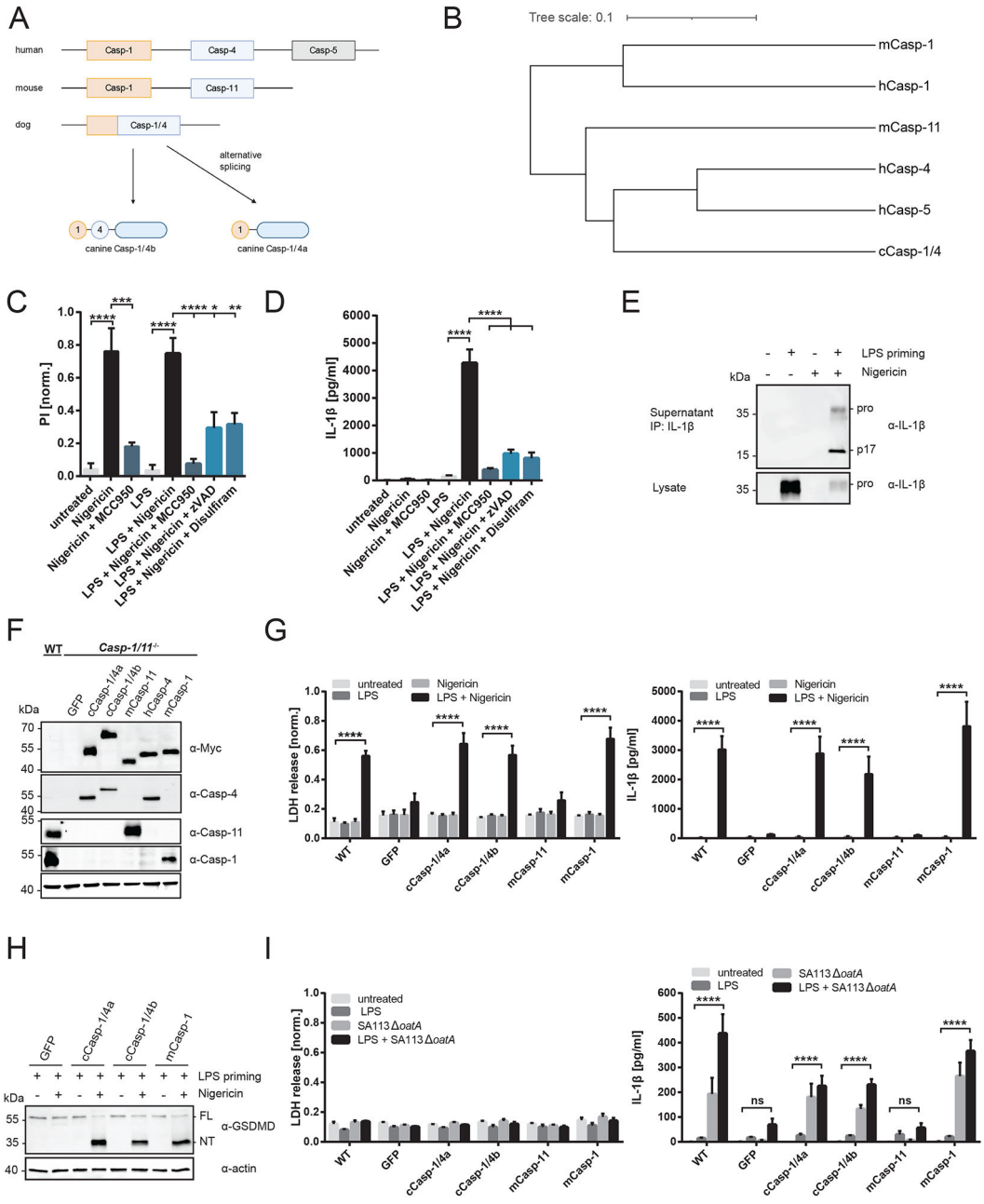

Fig. 1. Canine Casp-1/4 exhibit Casp-1 like inflammasome activities.

(A) Schematic of genetic loci encoding inflammatory caspases in humans, mice and dogs.

(B) Phylogenetic tree displaying evolutionary relationship between cCasp-1/4b and murine and human inflammatory caspases based on amino acid conservation.

(C-E) Canine primary MDMs were primed LPS for 4 h or left unprimed before stimulation with Nigericin for 3 h. Cells were pre-treated with indicated inhibitors for 30 min and inhibitors were co-administered during nigericin treatment. PI fluorescence intensity and cell-associated or extracellular IL-1β release was assessed after 3 h nigericin treatment.

(F) Immunoblot analysis of lysates of LPS-primed WT iBMDMs and *Casp-1/11*$^{-/-}$ iBMDMs reconstituted with the indicated Myc-tagged caspase.

(G) WT iBMDMs or *Casp-1/11*$^{-/-}$ iBMDMs reconstituted with the indicated caspase were primed for 4 h with LPS or left unprimed before treatment with nigericin for 3 h. LDH and IL-1β in supernatants were then quantified.

(H) *Casp-1/11*$^{-/-}$ iBMDMs reconstituted with indicated caspases were primed for 4 h with LPS, then either left untreated or stimulated with nigericin for 2 h. Lysates and media were combined to assess processing of GSDMD by immunoblot.

(I) WT iBMDMs or *Casp-1/11*$^{-/-}$ iBMDMs reconstituted with the indicated caspases were primed for 4 h with LPS or left unprimed before infection with *S. aureus* 113 Δ*oatA*. LDH and IL-1β in supernatants were quantified 12 h post-infection.

Data are represented as mean ± SEM of at least three independent experiments. Primary cell experiments include data from at least three different donors. Immunoblots show representative result of three independent repeats. Statistical significance was determined by one-way ANOVA (B+C) or two-way ANOVA (F+H): *p < 0.05; **p < 0.01; ***p < 0.001; ****p < 0.0001.

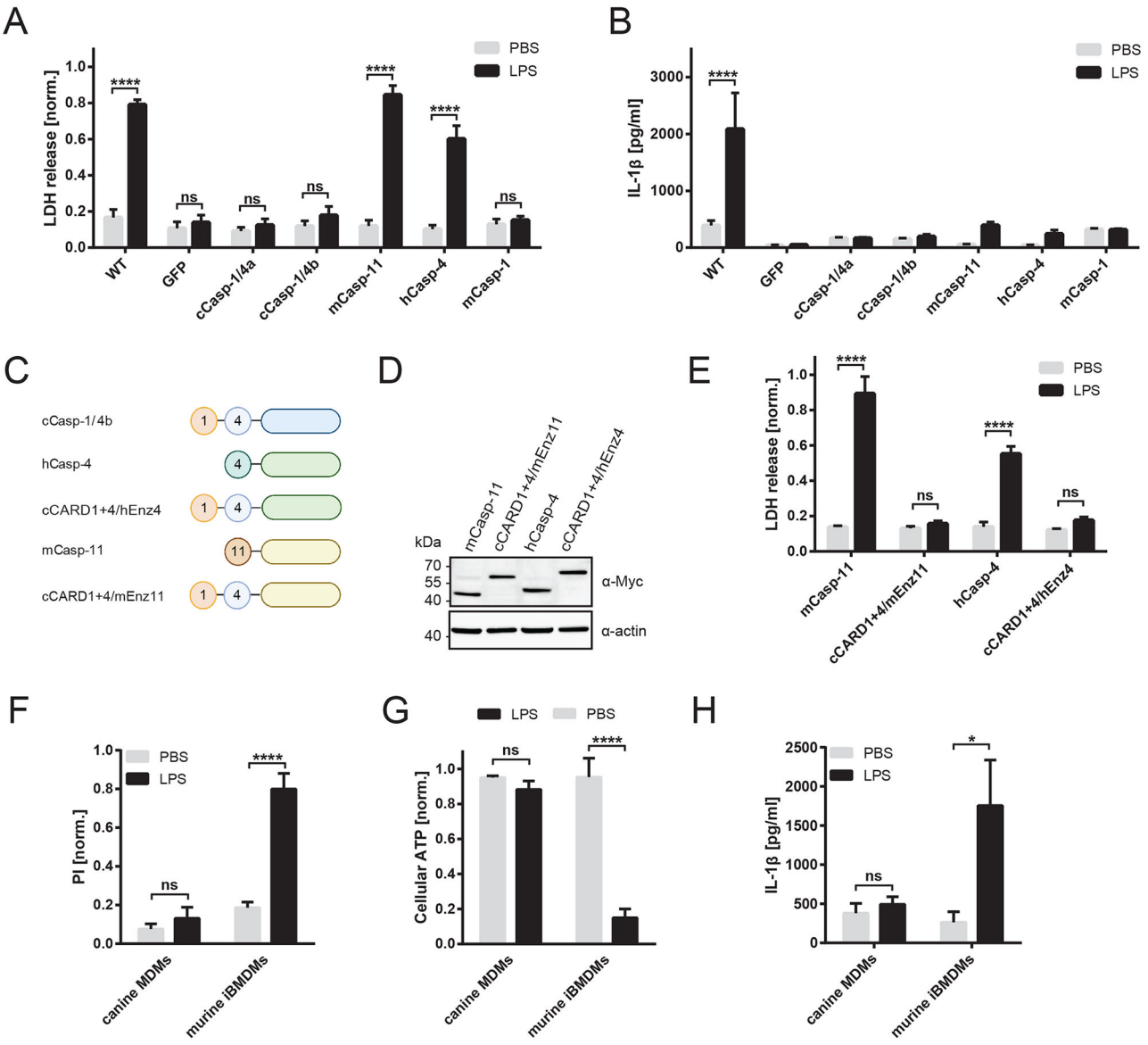

Fig. 2. Canine Casp-1/4 proteins do not act as cytosolic LPS sensors.

(A, B) WT iBMDMs or *Casp-1/11*$^{-/-}$ iBMDMs reconstituted with the indicated caspase were primed for 4 h with LPS before electroporation of LPS or PBS. LDH and IL-1β in supernatants was quantified after 3 h.

(C) Schematic of WT and chimeric caspase constructs.

(D) Immunoblot analysis of whole-cell lysates of *Casp-1/11*$^{-/-}$ iBMDMs reconstituted with the indicated Myc-tagged caspases.

(E) *Casp-1/11*$^{-/-}$ iBMDMs reconstituted with the caspases were primed for 4 h with LPS or left unprimed before electroporation of LPS or PBS. LDH in supernatants was quantified after 3 h.

(F-H) Canine primary MDMs or murine WT iBMDMs were primed with LPS for 4 h. LPS or PBS was delivered into the cytosol of the cells by electroporation. PI fluorescence intensity, intracellular ATP levels and IL-1β in supernatants were quantified after 3 h.

Data are represented as mean ± SEM of three (E), four (F-H), or five (A+B) independent experiments. Statistical significance was determined by two-way ANOVA: *$p < 0.05$; **$p < 0.01$; ***$p < 0.001$; ****$p < 0.0001$.

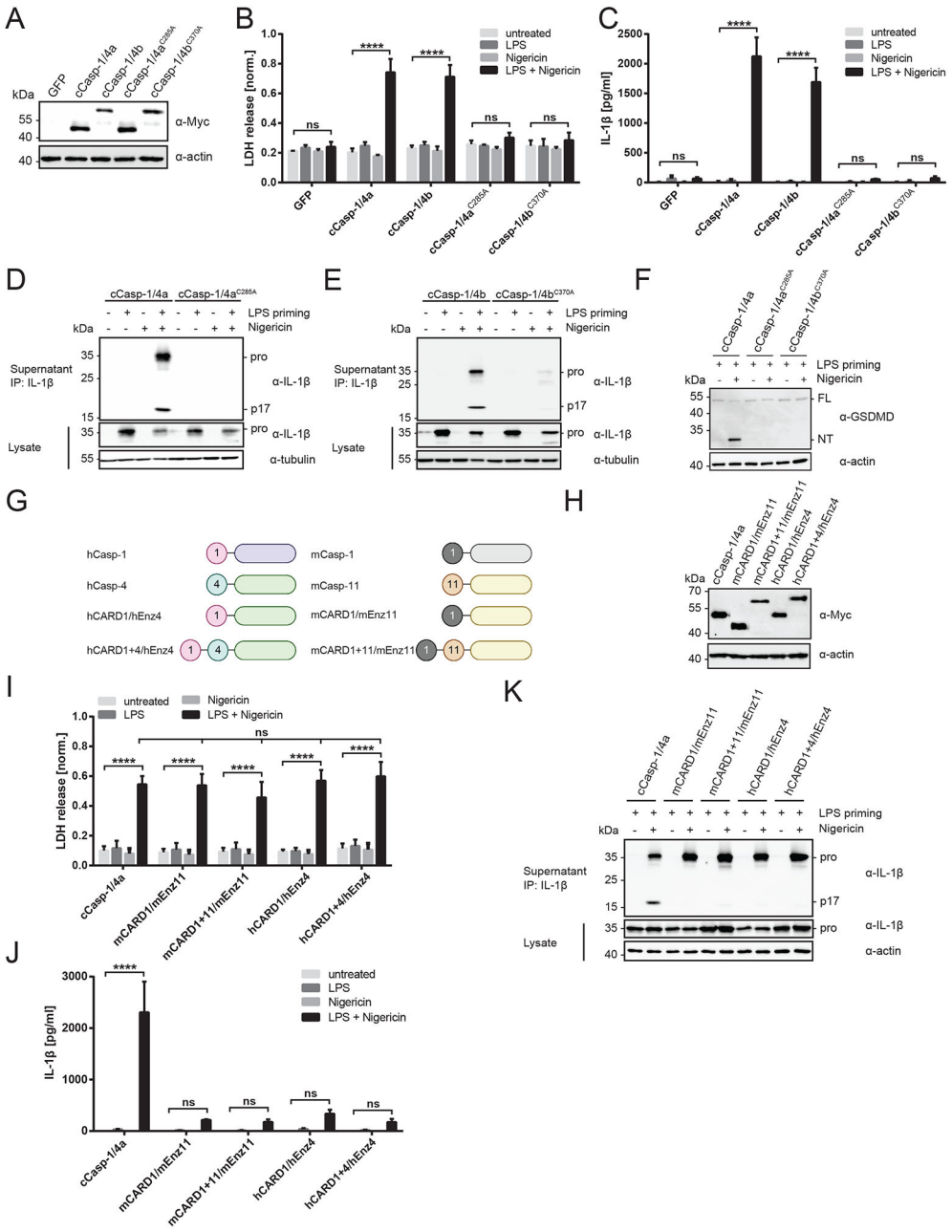

Fig. 3. The catalytic activity of cCasp-1/4 is required for inflammasome-dependent IL-1β release.

(A) Immunoblot analysis of lysates of *Casp-1/11*$^{-/-}$ iBMDMs expressing either Myc-tagged cCasp-1/4 variants.

(B-F) *Casp-1/11*$^{-/-}$ iBMDMs reconstituted with the indicated caspase were primed for 4 h with LPS or left unprimed before treatment with nigericin. LDH and intracellular and extracellular IL-1β were quantified after 3 h. Cells in (F) were treated with nigericin for 2 h before assessing GSDMD processing.

(G) Schematics showing architecture of synthetic hybrid caspases consisting of human or murine Casp-1 CARDs and the catalytic domains and CARDs of hCasp-4 or mCasp-11, respectively.

(H) Immunoblot analysis of lysates of *Casp-1/11*$^{-/-}$ iBMDMs expressing indicated Myc-tagged caspases.

(I-K) *Casp-1/11*$^{-/-}$ iBMDMs reconstituted with the caspases indicated were primed for 4 h with LPS or left unprimed before treatment with nigericin for 3 h. LDH and intracellular and extracellular IL-1β were then quantified.

Data are represented as mean ± SEM of three independent experiments. Immunoblots of immunoprecipitated IL-1β display one representative result of three independent repeats. Statistical significance was determined by two-way ANOVA: ****$p < 0.0001$.

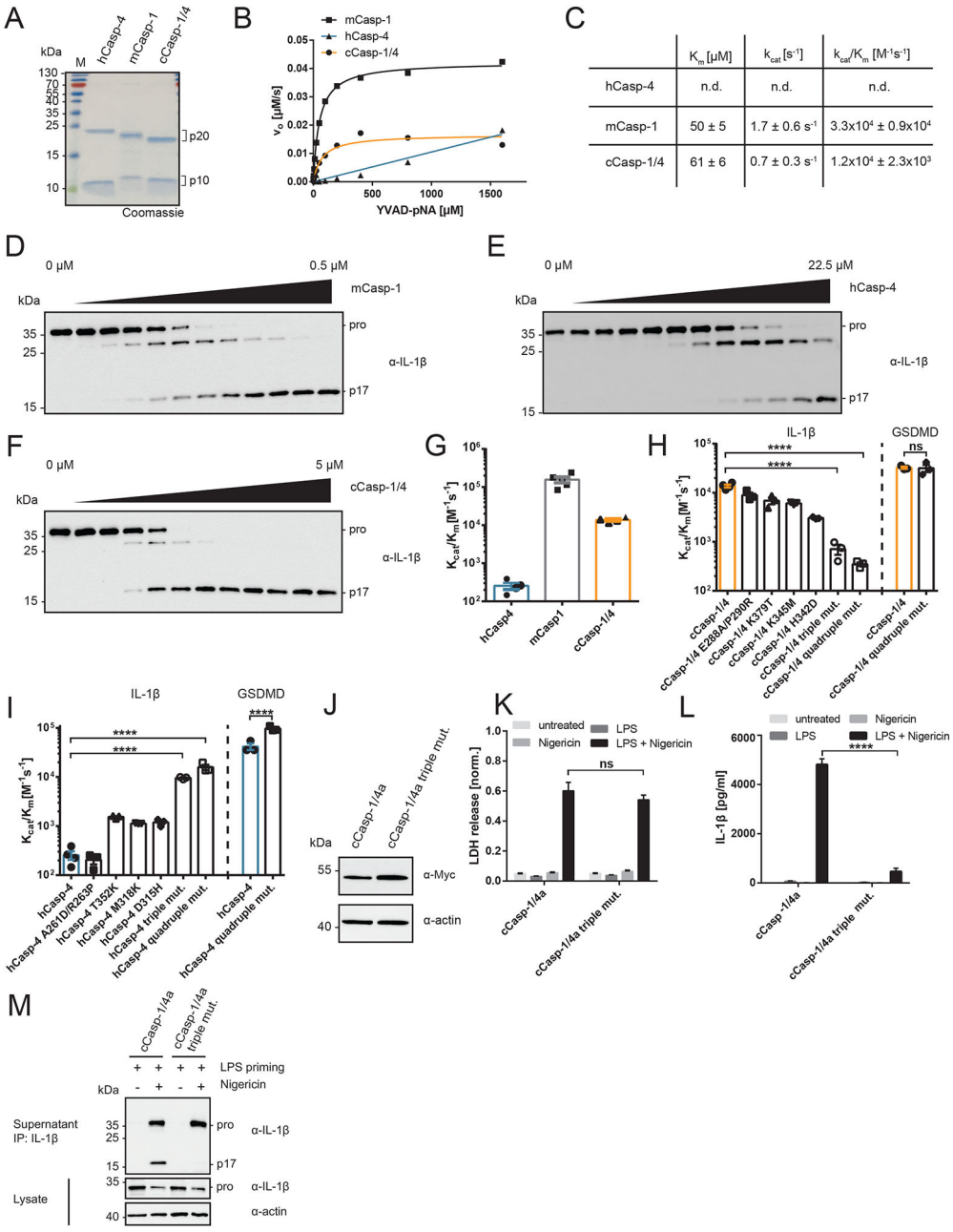

Fig. 4. Mechanistic insights in how inflammatory caspases select IL-1β as a substrate.

(A) Recombinant catalytic domains of the caspases indicated were visualized after SDS-PAGE by Coomassie staining.

(B, C) Enzyme kinetic analysis of the cleavage of the chromogenic Casp-1-substrate YVAD-pNA by recombinant caspases.

(B) Recombinant caspases (20 nM) were mixed with serially diluted substrate (0 – 1600 µM). Initial velocities were plotted in dependence of the substrate concentration and fitted according to the hyperbolic Michaelis-Menten equation to derive kinetic parameters.

(C) Calculated kinetic parameters of YVAD-pNA cleavage reaction for each tested caspase. Parameters for hCasp-4 could not be accurately determined as curves did not reach

saturation in the tested range of substrate concentrations. Displayed parameters represent mean ± SD of three independent experiments involving two separate caspase preparations.
(D-G) 50 nM of recombinant murine pro-IL-1β was incubated with two-fold serial dilutions of caspase catalytic domains. Processing of pro-IL-1β was analyzed by immunoblot. Highest enzyme concentration used in each assay is indicated above the blot. Catalytic efficiencies (k_{cat}/K_m) were calculated based on disappearance of band corresponding to pro-form of IL-1β.
(H) Catalytic efficiencies of pro-IL-1β and GSDMD cleavage by cCasp-1/4 mutants. Triple mutant carries K379T, K345M and H342D mutations. Quadruple mutant combines these three mutations with E288A/P290R mutation.
(I) Catalytic efficiencies of pro-IL-1β and GSDMD cleavage by hCasp-4 mutants. Triple mutant carries T352K, M318K and D315H mutations. Quadruple mutant combines these three mutations with A261E/R263P mutation.
(J) Immunoblot analysis of whole-cell lysates of *Casp-1/11*$^{-/-}$ iBMDMs expressing Myc-tagged caspases indicated.
(K - M) *Casp-1/11*$^{-/-}$ iBMDMs reconstituted with cCasp-1/4a or cCasp-1/4a triple mutant were primed for 4 h with LPS or left unprimed before treatment with nigericin for 3 h. LDH and intracellular and extracellular IL-1β were then quantified.
Each data point (G-I) represents the result of one independent assay. Bars and error bars represent mean ± SEM of at least three independent experiments. Repeats of *in vitro* assays involved at least two independent caspase preparations. Immunoblots are representative of at least three independent repeats. Statistical significance was determined by one-way ANOVA (H, I) or two-way ANOVA (K, L): ****$p < 0.0001$.

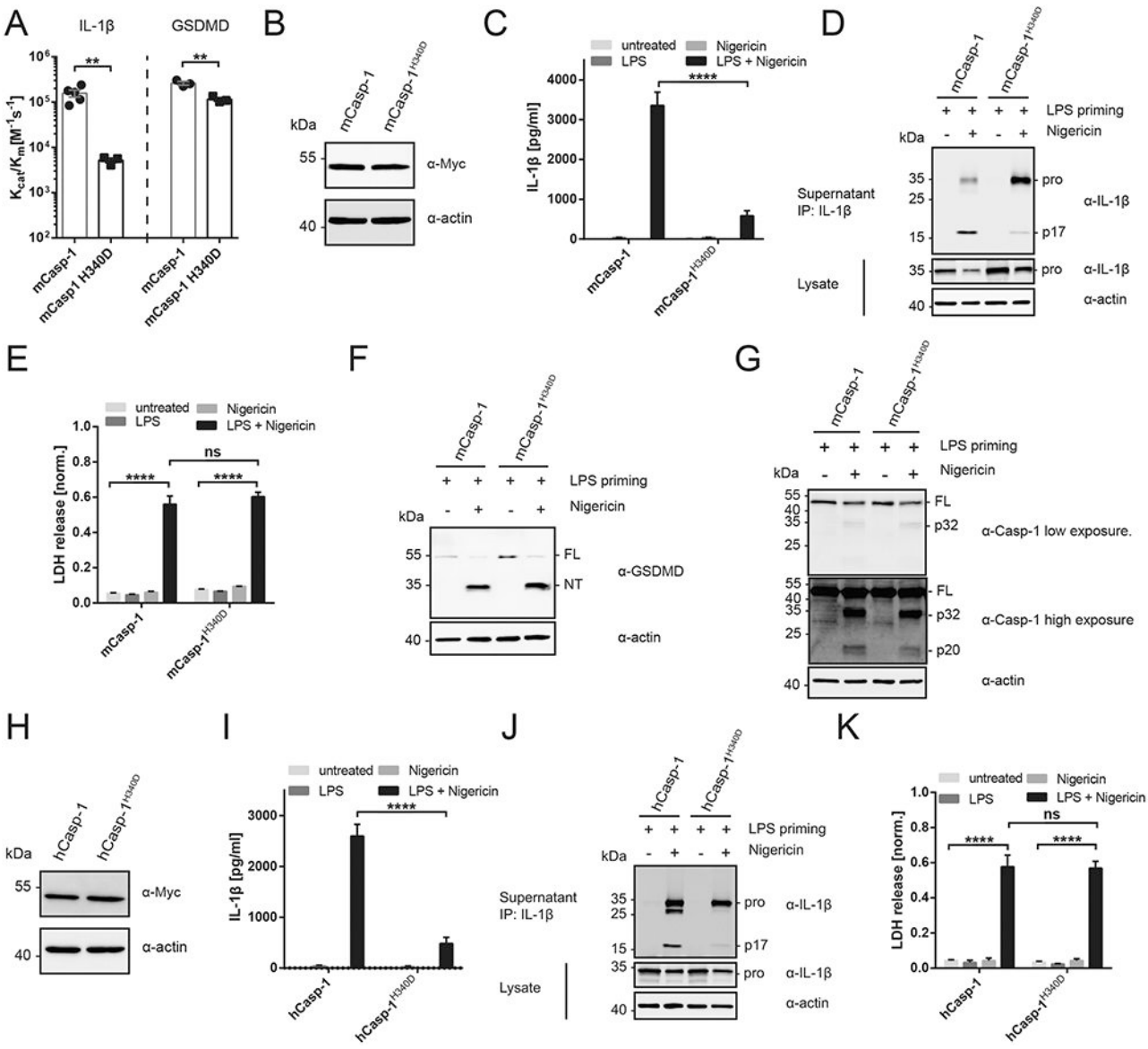

Fig. 5. The conserved residue H340 determines ICE activity in Caspase-1.

(A) Catalytic efficiencies of pro-IL-1β and GSDMD cleavage by mCasp-1 H340D compared to WT mCasp-1.

(B, H) Immunoblot analysis of lysates of *Casp-1/11*$^{-/-}$ iBMDMs expressing the indicated Myc-tagged caspases.

(C – G, I - K) *Casp-1/11*$^{-/-}$ iBMDMs expressing the caspases indicated were primed for 4 h with LPS or left unprimed before treatment with nigericin for 3 h. LDH and intracellular and extracellular IL-1β or GSDMD cleavage status were then quantified.

Each data point (A) represents the result of one independent assay. Bars and error bars represent mean ± SEM of at least three independent experiments. Repeats of *in vitro* assays involved at least two independent caspase preparations. Immunoblots are representative of at least three independent repeats. Statistical significance was determined by one-way ANOVA (A) or two-way ANOVA (C, E, I, K): ****$p < 0.0001$.

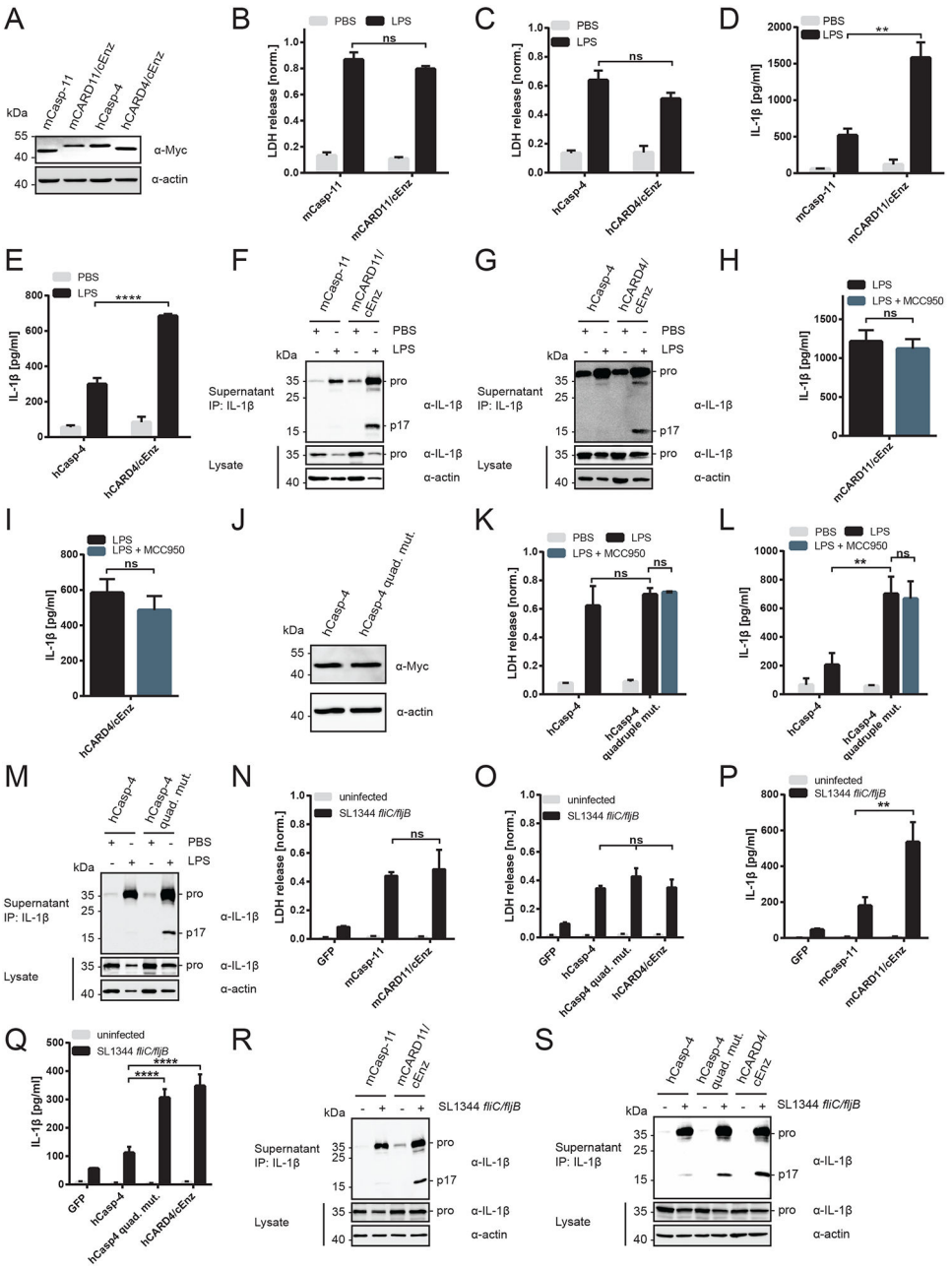

Fig. 6. Design of a synthetic one-protein signaling pathway that links LPS detection and IL-1β release, independent of inflammasomes.

(A, J) Immunoblot analysis of lysates of *Casp-1/11*$^{-/-}$ iBMDMs expressing the indicated Myc-tagged caspases.

(B-I, K-M) *Casp-1/11*$^{-/-}$ iBMDMs reconstituted with the indicated caspase were primed for 4 h with LPS before electroporation of LPS or PBS. LDH and intracellular and extracellular IL-1β were assessed after 3 h. As indicated, the NLRP3 inhibitor MCC950 was added after electroporation.

(N-S) *Casp-1/11*$^{-/-}$ iBMDMs reconstituted with the indicated caspase were primed for 3 h with LPS before infection with *Salmonella*. LDH release and IL-1β in supernatants were

quantified after 4 h. Immunoprecipitated IL-1β from supernatants and pro-IL-1β in lysates were analyzed by immunoblotting after 4 h.

Data are represented as mean ± SEM of three independent experiments. Immunoblots of immunoprecipitated IL-1β are representative of three independent repeats. Statistical significance was determined by unpaired Student's t-test (H, I) or two-way ANOVA (B, C, D, E, K, L, N, O, P, Q): *$p < 0.05$; **$p < 0.01$; ***$p < 0.001$; ****$p < 0.0001$.

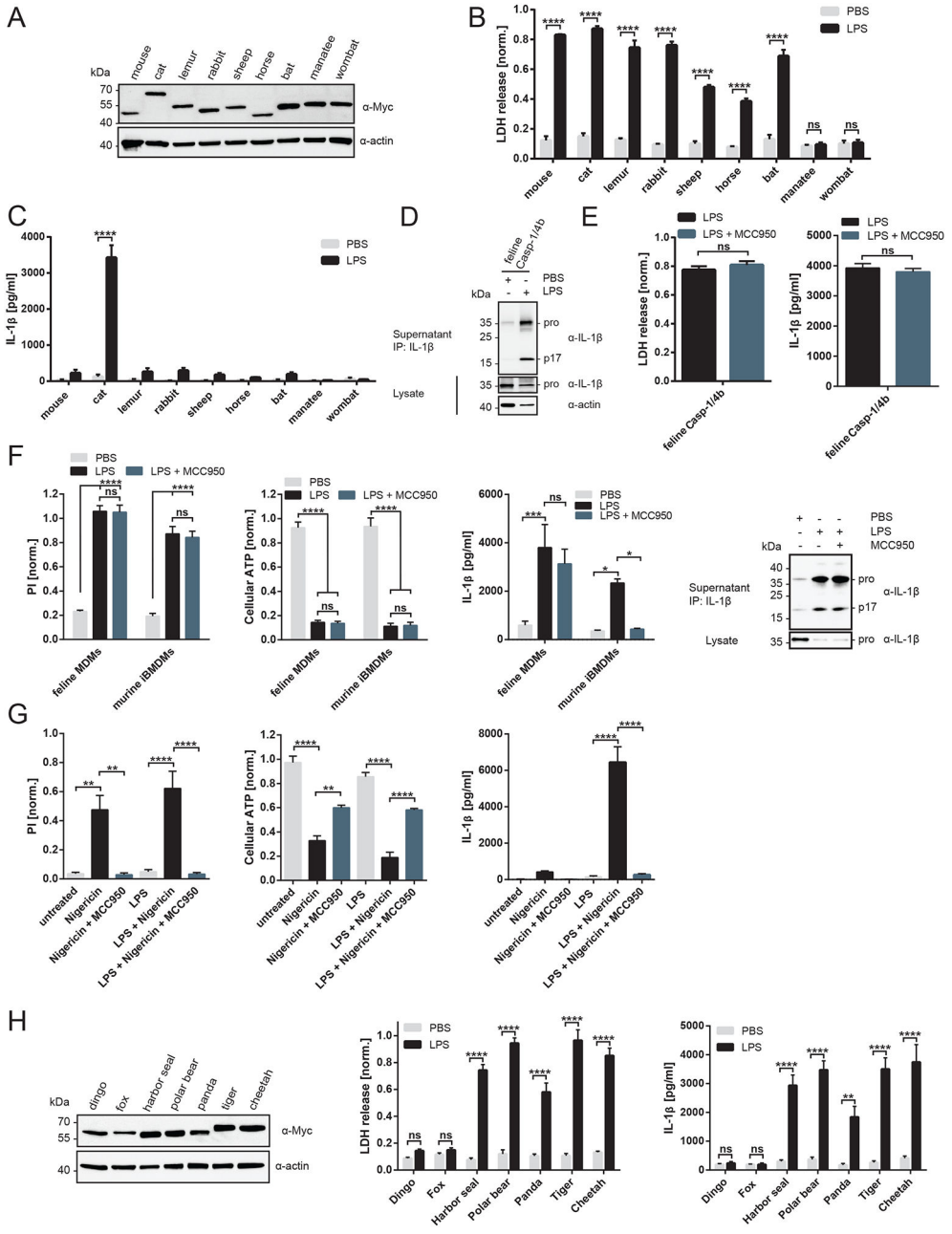

Fig. 7. Multiple animal species contain a natural one-protein signaling pathway that links LPS detection to IL-1β cleavage.

(A) Immunoblot analysis of lysates from *Casp-1/11*$^{-/-}$ iBMDMs reconstituted with Myc-tagged Casp-4 homologues from following species: mouse (*Mus musculus*), cat (*Felis catus*), lemur (*Microcebus murinus*), rabbit (*Oryctolagus cuniculus*), sheep (*Ovis aries*), horse (*Equus caballus*), bat (*Pteropus alecto*), manatee (*Trichechus manatus latirostis*), wombat (*Wombatus ursinus*).

(B-E) *Casp-1/11*$^{-/-}$ iBMDMs reconstituted with the casp-4 homologue from the indicated species were primed for 4 h with LPS before electroporation of LPS or PBS. LDH and

intracellular and extracellular IL-1β were then assessed. after 3 h. As indicated, the NLRP3 inhibitor MCC950 was added after electroporation.

(F) Feline primary MDMs or murine iBMDMs were primed with LPS for 4 h. Subsequently, LPS or PBS was delivered into the cytosol by electroporation. PI fluorescence intensity, intracellular ATP, and extracellular and intracellular IL-1β were assessed 3 h post-electroporation. As indicated, the NLRP3 inhibitor MCC950 was present in media after electroporation.

(G) Feline primary MDMs were primed with LPS for 4 h or left unprimed before stimulation with nigericin. Cells were pre-treated with MCC950 for 30 min and inhibitor was co-administered during nigericin treatment. PI fluorescence intensity, intracellular ATP levels, and extracellular IL-1β were quantified after 3 h.

(H) *Casp-1/11*$^{-/-}$ iBMDMs were reconstituted with Myc-tagged Casp-1/4b homologues from following carnivorans: dingo (*Canis lupus dingo*), fox (*Vulpes vulpes*), harbor seal (*Phoca vitulina*), polar bear (*Ursus maritimus*), panda (*Ailuropoda melanoleuca*), tiger (*Panthera tigris altaica*), cheetah (*Acinonyx jubatus*). Cells were primed for 4 h with LPS before electroporation of LPS or PBS. LDH release and IL-1β levels in supernatants were quantified after 3 h.

Data are represented as mean ± SEM of at least three independent experiments.

Primary cell experiments include data from three different donors. Immunoblots of immunoprecipitated IL-1β are representative of three independent repeats. Statistical significance was determined by two-way ANOVA (B,C,F,H), unpaired Student’s t-test (E) or one-way ANOVA (G): *p < 0.05; **p < 0.01; ***p < 0.001; ****p < 0.0001.